Natural variation in arsenic toxicity is explained by differences in branched chain amino acid catabolism

Stefan Zdraljevic[1,2], Bennett W. Fox[3], Christine Strand[5], Oishika Panda[3,4], Francisco J. Tenjo[3,4], Shannon C. Brady[1,2], Tim A. Crombie[2], John G. Doench[5], Frank C. Schroeder[3], and Erik C. Andersen[1,2,6] *

1. Interdisciplinary Biological Sciences Program, Northwestern University, Evanston, IL 60208, USA
2. Department of Molecular Biosciences, Northwestern University, Evanston, IL 60208, USA
3. Boyce Thompson Institute and Department of Chemistry and Chemical Biology, Cornell University, Ithaca, NY 14853, USA
4. The Buck Institute for Research on Aging, Novato, CA 94945, USA
5. Broad Institute of MIT and Harvard, Cambridge, MA 02142, USA
6. Robert H. Lurie Comprehensive Cancer Center of Northwestern University, Chicago, IL 60611, USA
* Corresponding author

Erik C. Andersen
Assistant Professor of Molecular Biosciences
Northwestern University
Evanston, IL 60208, USA
Tel: (847) 467-4382
Fax: (847) 491-4461
Email: Erik.Andersen@Northwestern.edu

Stefan Zdraljevic, stefanzdraljevic2018@u.northwestern.edu, ORCID 0000-0003-2883-4616
Bennett William Fox, bwf7@cornell.edu, ORCID 0000-0002-9749-3491
Christine Strand, cstrand@broadinstitute.org, ORCID 0000-0001-5783-6667
Oishika Panda, op56@cornell.edu, ORCID 0000-0002-1217-8231
Francisco J. Tenjo, fjt38@cornell.edu, 0000-0003-4848-916X
Shannon C. Brady, shannonbrady2014@u.northwestern.edu, ORCID 0000-0002-3043-1544
Tim A. Crombie, tcrombie@northwestern.edu, ORCID 0000-0002-5645-4154
John G. Doench, jdoench@broadinstitute.org, ORCID 0000-0002-3707-9889
Frank C. Schroeder, fs31@cornell.edu, ORCID 0000-0002-4420-0237
Erik Andersen, erik.andersen@northwestern.edu, ORCID 0000-0003-0229-9651

Abstract

Organisms are often exposed to the environmentally ubiquitous toxic metalloid arsenic, and genetic differences unique to individuals can cause differential susceptibility to arsenic. To understand how molecular mechanisms of arsenic toxicity vary among individuals, we used two genetic mapping approaches to show that a major source of natural differences in *Caenorhabditis elegans* responses to arsenic trioxide is caused by variation in the *dbt-1* gene. This gene encodes the E2 subunit of the branched-chain α-keto acid dehydrogenase (BCKDH) complex, a core component of branched-chain amino acid (BCAA) catabolism. We used CRISPR/Cas9-mediated genome editing to show that a single non-synonymous variant (C78S) in the highly conserved lipoyl domain of DBT-1 is the causal polymorphism underlying variation in response to arsenic trioxide. Using targeted metabolomics and chemical supplementation experiments, we demonstrate that differences in *C. elegans* responses to arsenic trioxide are caused by variation in the abundances of iso-branched chain fatty acids that serve a central role in developmental progression. We hypothesize that the presence of the additional thiol group in the sensitive DBT-1 C78 allele participates in arsenic binding, thereby more strongly inhibiting BCKDH function. We go on to show that branched chain fatty acids are affected after arsenic treatment of human cells. This finding has broad implications for arsenic toxicity and for arsenic-focused chemotherapeutics across divergent individuals in human populations. Our study implicates the BCKDH complex and BCAA metabolism in arsenic responses, demonstrating the power of using *C. elegans* natural genetic diversity in combination with comparative metabolomics to identify mechanisms by which environmental toxins affect organismal physiology.

Introduction

An estimated 100 million people are currently at risk of chronic exposure to arsenic, a toxic metalloid that can be found in the environment (Ravenscroft, Brammer, and Richards 2009). The high prevalence of environmental arsenic and the severe toxicity associated with arsenic exposure has made it the number one priority for the United States Agency for Toxic Substances and Disease Registry (https://www.atsdr.cdc.gov/SPL/). Inorganic trivalent arsenic As(III) compounds, which include arsenic trioxide (As_2O_3), are the most toxic forms of environmental arsenic (Ratnaike 2003; Mandal and Suzuki 2002). In humans, As(III) is detoxified by methylation to the least toxic dimethylarsenite (DMA) form (Khairul et al. 2017; Stýblo et al. 2002). However, this methylation process also creates the highly toxic monomethylarsenite (MMA) form, so ratios of DMA to MMA determine levels of arsenic toxicity. Both MMA and DMA are produced from As(III) via the arsenic methyltransferase (AS3MT) (Schlebusch et al. 2015). Interestingly, individuals from human subpopulations that inhabit high arsenic environments have higher DMA/MMA ratios than individuals from low-arsenic environments. The elevated DMA/MMA ratio in individuals from high-arsenic environments is associated with natural differences in the *AS3MT* gene (Chung et al. 2009; Fujihara et al. 2009; Gomez-Rubio et al. 2010), which shows signs of strong positive selection. These results suggest that a more active AS3MT enzyme in these human subpopulations makes more DMA and enables adaptation to elevated environmental arsenic levels (Schlebusch et al. 2015). Importantly, population-wide differences in responses to environmental arsenic cannot be explained solely by variation in *AS3MT*, indicating that other genes must impact arsenic toxicity.

Despite its toxicity, arsenic trioxide has been used as a therapeutic agent for hundreds of years. Most recently, it was introduced as a highly effective cancer chemotherapeutic for the treatment of acute promyelocytic leukemia (APL) (Chen et al. 1997; Antman 2001; Murgo 2001; Emi 2017). Hematopoietic differentiation and apoptosis in APL patients is blocked at the level of promyelocytes by the Promyelocytic Leukemia/Retinoic Acid Receptor alpha fusion protein caused by a t(15;17) chromosomal translocation (de Thé et al. 1990; Grignani et al. 2000). Arsenic trioxide has been shown to directly bind a cysteine-rich region of the RING-B box coiled-coil domain of PML-RARα, which causes the degradation of the oncogenic fusion protein (Zhang et al. 2010; Tomita, Kiyoi, and Naoe 2013). The success of arsenic trioxide (Trisenox®) has spurred its use in over a hundred clinical trials in the past decade (Hoonjan, Jadhav, and Bhatt 2018). Despite these successes, individual differences in the responses to arsenic-based treatments, including patient-specific dosing regimens and side effects, limit the full therapeutic benefit of this compound (Zeidan and Gore 2014). Medical practitioners require knowledge of the molecular mechanisms for how arsenic causes toxicity to provide the best individual-based therapeutic benefits.

Studies of the free-living roundworm *Caenorhabditis elegans* have greatly facilitated our understanding of basic cellular processes (Kniazeva et al. 2004; Luz et al. 2017; Spracklin et al. 2017; Watson et al. 2013), including a number of studies that show that the effects of arsenic are similar to what is observed in mammalian model systems and humans. These effects include mitochondrial toxicity (Luz and Meyer 2016; Luz et al. 2016), the generation of reactive oxygen species (ROS) (Schmeisser et al. 2013), genotoxicity (Wyatt et al. 2017), genome-wide shifts in chromatin structure (Large et al. 2016), reduced lifespan (Schmeisser et al. 2013), and

induction of the heat-shock response (Wang et al. 2017). However, these studies were all performed in the genetic background of the standard *C. elegans* laboratory strain (N2). To date, 152 *C. elegans* strains have been isolated from various locations around the world (Andersen et al. 2012; Cook, Zdraljevic, Tanny, et al. 2016; Cook, Zdraljevic, Roberts, et al. 2016), which contain a largely unexplored pool of genetic diversity much of which could underlie adaptive responses to environmental perturbations (Zdraljevic and Andersen 2017).

We used two quantitative genetic mapping approaches to show that a major source of variation in *C. elegans* responses to arsenic trioxide is caused by natural variation in the *dbt-1* gene, which encodes an essential component of the highly conserved branched-chain α-keto acid dehydrogenase (BCKDH) complex (Jia et al. 2016). The BCKDH complex is a core component of branched-chain amino acid (BCAA) catabolism, which has not been previously implicated in arsenic responses. Furthermore, we show that a single missense variant in DBT-1(S78C), located in the highly conserved lipoyl-binding domain, underlies phenotypic variation in response to arsenic. Using targeted and untargeted metabolomics and chemical rescue experiments, we show that differences in wild isolate responses to arsenic trioxide are caused by differential synthesis of mono-methyl branched chain fatty acids (mmBCFA), metabolites with a central role in development (Kniazeva et al. 2004). These results demonstrate the power of using the natural genetic diversity across the *C. elegans* species to identify mechanisms by which environmental toxins affect physiology.

Results

Natural variation on chromosome II underlies differences in arsenic responses

We quantified arsenic trioxide sensitivity in *C. elegans* using a high-throughput fitness assay that utilizes the COPAS BIOSORT (Andersen et al. 2015; Zdraljevic et al. 2017). In this assay, three L4 larvae from each strain were sorted into arsenic trioxide or control conditions. After four days of growth, we measured the brood size and progeny lengths of these animals using the BIOSORT. We defined brood size as the total number of objects detected by the BIOSORT and progeny length by the median of individual progeny time-of-flight (TOF) measurements. To identify an appropriate concentration of arsenic trioxide for linkage and GWA mapping assays, we performed dose-response experiments on four genetically diverged isolates of *C. elegans*: N2, CB4856, JU776, and DL238 (Figure S1A). When compared to control conditions, all four strains produced fewer progeny at all arsenic trioxide concentrations, whereby the lowest concentration at which we observed a significant reduction in brood size for all strains was 1 mM. In addition to reduced brood sizes, we observed that the progeny of animals exposed to arsenic trioxide were shorter in length than the progeny of animals grown in control conditions, which indicates an arsenic-induced developmental delay (Figure S1B). We found that CB4856 animals produced approximately 16% more offspring that were on average 20% larger than JU775, DL238, and N2 animals when treated with 1 mM arsenic trioxide, suggesting that the CB4856 strain was more resistant to arsenic trioxide than the other three strains.

The increased arsenic trioxide resistance of CB4856 compared to N2 motivated us to perform linkage mapping experiments with a panel of recombinant inbred advanced intercross lines (RIAILs) that were previously constructed through ten generations of intercrossing

between an N2 derivative (QX1430) and CB4856 (Andersen et al. 2015). To capture arsenic trioxide-induced phenotypic differences in brood size and progeny length, we exposed a panel of 252 RIAILs to 1 mM arsenic trioxide. For both traits, we corrected for growth differences among RIAILs in control conditions and assay-to-assay variability using linear regression (see Materials and Methods). Linkage mapping analysis revealed that arsenic trioxide-induced variation in RIAIL brood size and progeny length are significantly associated with genetic variation on the center of chromosome II (Figure 1A). The brood-size quantitative trait locus (QTL) explains 9.4% of the variation in brood size among strains in the RIAIL panel, and the confidence interval spans from 6.04 to 9.30 Mb on chromosome II. This QTL completely encompasses the progeny-length QTL, which has a confidence interval spanning from 6.82 to 8.93 Mb on chromosome II and explains 24.9% of the variation in progeny length among the RIAILs. Matching our observations from the dose-response experiments, RIAILs with the CB4856 genotype at the peak marker for these QTL had larger brood sizes and longer progeny in the presence of arsenic trioxide than recombinant lines with the N2 genotype (Figure S2A-B). Because the confidence intervals of these QTL overlap, variation in brood size and progeny length in the RIAIL panel could be affected by the same genetic variant(s). However, each of these QTL confidence intervals span genomic regions greater than two megabases and contain hundreds of genes that vary between N2 and CB4856 (brood size: 567, progeny length: 373). Therefore, we constructed near-isogenic lines (NILs) to isolate and narrow each QTL in a controlled genetic background.

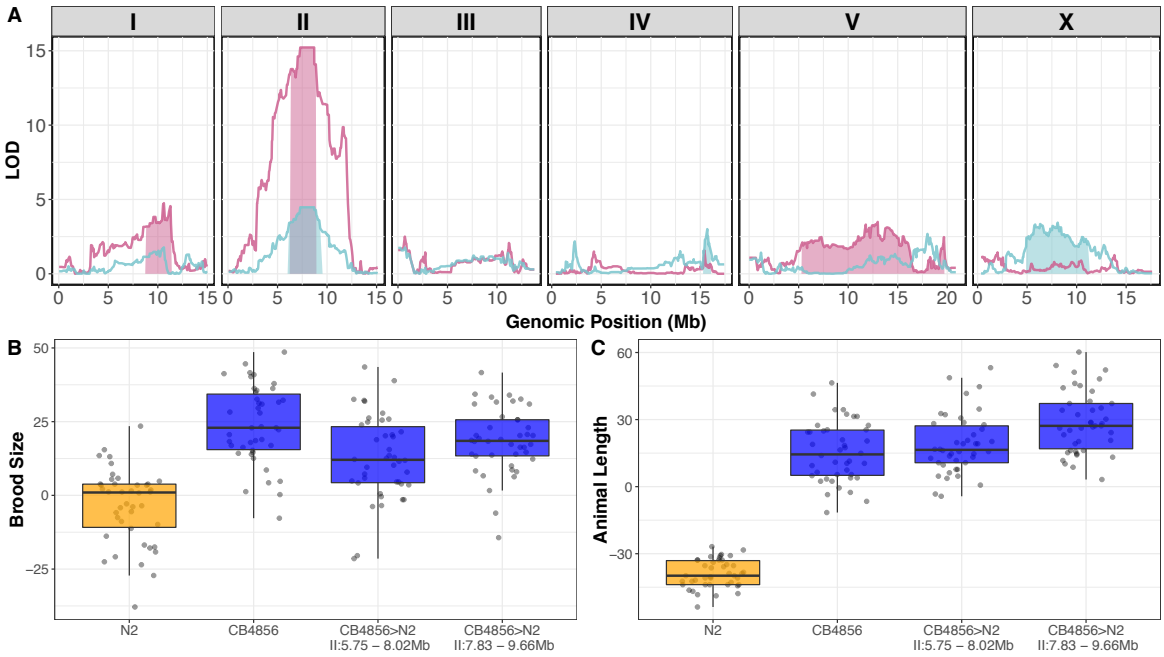

Figure 1: A large-effect QTL on the center of chromosome II explains differences in arsenic trioxide response between N2 and CB4856

(A) Linkage mapping plots for regressed brood size (teal) and median animal length (pink) in the presence of arsenic trioxide are shown. The significance values (logarithm of odds, LOD, ratio) for 1454 markers between the N2 and CB4856 strains are on the y-axis, and the genomic position (Mb) separated by chromosome is plotted on the x-axis. The associated 1.5 LOD-drop confidence intervals are represented by teal and pink boxes for brood size and median animal length, respectively. Tukey box plots of near-isogenic line (NIL) phenotype values for regressed (B) brood size and (C) median animal

length in the presence of arsenic trioxide are shown. NIL genotypes are indicated below the plot as genomic ranges. The N2 brood sizes and progeny lengths are significantly different from all other strains (Brood size: Tukey HSD *p*-value < 1.56E-7; Animal Length: Tukey HSD *p*-value < 3.0E-14).

To split the large QTL confidence intervals in half, we introgressed genomic regions from the CB4856 strain on the left and right halves of the confidence intervals into the N2 genetic background. In the presence of arsenic trioxide, both of these NILs had similar brood sizes and progeny of similar length as the CB4856 parental strain (Figure 1B and C). The phenotypic similarity of these NILs to the CB4856 parental strain suggested that the two NILs might share an introgressed region of the CB4856 genome. To identify this shared introgressed region, we performed low-coverage sequencing of the NIL strains and defined the left and right bounds of the CB4856 genomic introgression to be from 5.75 to 8.02 Mb and 7.83 to 9.66 Mb in the left and right NILs, respectively (Supplemental table 9). Taken together, these results strongly suggested that genetic differences between N2 and CB4856 within 7.83 to 8.02 Mb on chromosome II conferred resistance to arsenic trioxide.

In parallel to the linkage-mapping approach described above, we performed a genome-wide association (GWA) mapping experiment by quantifying the responses to arsenic trioxide for 86 wild *C. elegans* strains (Andersen et al. 2012). We found no significant QTL associated with brood size nor progeny length measurements with this approach. However, the GWA experiment we performed had lower statistical power to detect QTL than the linkage mapping experiment, because we only tested 86 strains in single replicates. To circumvent this issue, we performed principal component analysis (PCA) on all traits measured by the COPAS BIOSORT and post-processed using the *easysorter* R package (Andersen et al. 2015). In total, 67 processed phenotype measurements were included in the PCA. This analysis revealed that eight principal components (PCs) explain more than 95% of the variation in the data set, and the first PC alone captures approximately 68% of the variation in the data set (Figure S3). Closer inspection of the first PC indicates that it is highly correlated with the progeny length trait, median TOF (r = 0.89, p-value = 4.7E-31) (Figure S4). We therefore considered the first PC as a progeny length-related phenotype for GWA mapping. Variation in the first PC among the wild isolates mapped to a QTL on the center of chromosome II that spans from 7.43 Mb to 8.33 Mb (Figure 2A). This QTL overlaps with the QTL identified by linkage mapping and follow-up NIL experiments, which suggested to us that the same causal genetic variant(s) underlies both QTL. Additionally, strains with the non-reference genotype at the peak SNV from the PC mapping tended to have higher PC1 values, which correlated with longer progeny lengths, than strains with the reference genotype when exposed to arsenic trioxide (Figure 2B). These results matched our observations that RIAILs with the CB4856 genotype at the QTL marker tended to be more resistant to arsenic trioxide than RIAILs with the N2 genotype at the QTL marker, further supporting that the QTL we identified by linkage and GWA mapping might be caused by the same underlying genetic variants. To explore this hypothesis further, we performed fine mapping within the PC1 QTL confidence interval identified by GWA mapping.

To fine map the PC1 QTL, we focused on variants from the *C. elegans* whole-genome variation dataset (Cook, Zdraljevic, Tanny, et al. 2016) that are shared among at least five percent of the 86 wild isolates exposed to arsenic trioxide. Under the assumption that the linkage and GWA mapping QTL are caused by the same genetic variation, we also considered variants present in the CB4856 strain. We calculated the *p*-value of Spearman's *rho* correlation

coefficients between the first PC and each single-nucleotide variant (SNV) in the QTL confidence interval (Figure 2C). From this analysis, we found that a single SNV is highly correlated with the arsenic trioxide response ($-log_{10}(p) = 6.05$). It affects the *dbt-1* gene, which results in a cysteine to serine missense variant at position 78 (C78S) of DBT-1. This highly correlated variant is also present in the NIL-defined QTL that spans from 7.83 to 8.02 Mb on chromosome II.

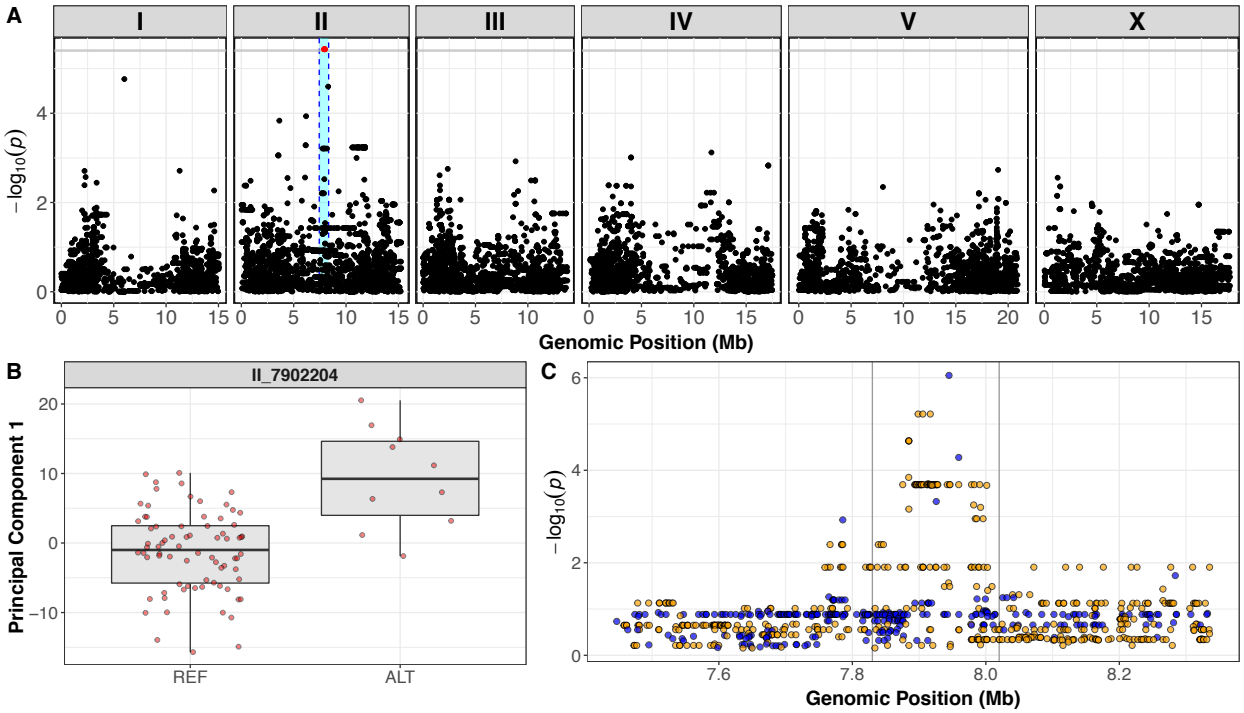

Figure 2: GWA mapping results of the first principal component
A) A manhattan plot for the first principal component in the presence of arsenic trioxide is shown. Each dot represents an SNV that is present in at least 5% of the assayed wild population. The genomic position in Mb, separated by chromosome, is plotted on the x-axis and the $-log_{10}(p)$ for each SNV is plotted on the y-axis. SNVs are colored red if they pass the genome-wide Bonferroni-corrected significance threshold, which is denoted by the gray horizontal line. The genomic region of interest surrounding the QTL is represented by a cyan rectangle. (B) Tukey box plots of phenotypes used for association mapping in (A) are shown. Each dot corresponds to the phenotype of an individual strain, which is plotted on the y-axis. Strains are grouped by their genotype at the peak QTL position (red SNV from panel A, ChrII:7,902,204), where REF corresponds to the allele from the reference N2 strain. (C) Fine mapping of the chromosome II region of interest, showing the calculated *p*-value associated with the Spearman's *rho* statistic for every variant present in the QTL confidence interval from (A) is shown. Blue dots correspond to variants that are present in the CB4856 strain, and orange dots correspond to variants that are present in the rest of the wild population.

A cysteine-to-serine variant in DBT-1 contributes to arsenic response variation

The *C. elegans dbt-1* gene encodes the E2 component of the branched-chain α-keto acid dehydrogenase complex (BCKDH) (Jia et al. 2016). The BCKDH complex is a core component of branched-chain amino acid (BCAA) catabolism and catalyzes the irreversible oxidative decarboxylation of amino acid-derived branched-chain α-ketoacids (Adeva-Andany et al. 2017). The BCKDH complex belongs to a family of α-ketoacid dehydrogenases that includes

pyruvate dehydrogenase (PDH) and α-ketoglutarate dehydrogenase (KGDH) (Bergquist et al. 2009). All three of these massive enzymatic complexes include a central E2 component that is lipoylated at one critical lysine residue (two residues in PDH). The function of these enzymatic complexes depends on the lipoylation of these lysine residues (Bergquist et al. 2009; Reed and Hackert 1990). In *C. elegans*, the putative lipoylated lysine residue is located at amino acid position 71 of DBT-1, which is in close proximity to the C78S residue that we found to be highly correlated with arsenic trioxide resistance.

To confirm that the C78S variant in DBT-1 contributes to differential arsenic trioxide responses, we used CRISPR/Cas9-mediated genome editing to generate allele-replacement strains by changing the C78 residue in the N2 strain to a serine and the S78 residue in the CB4856 strain to a cysteine. Arsenic trioxide treatment of these strains revealed that the N2 DBT-1(S78) allele-replacement strain had increased resistance to arsenic trioxide, as measured by brood size (Figure 3A) and progeny lengths (Figure 3B), when compared to the parental N2 DBT-1(C78) strain. Conversely, the CB4856 DBT-1(C78) allele-replacement strain had decreased resistance to arsenic trioxide, as measured by brood size (Figure 3A) and progeny lengths (Figure 3B), when compared to the parental CB4856 DBT-1(S78) strain. We obtained the same result when we used the first PC from principal component analysis as a trait (Figure S5). When considering brood size, the N2 DBT-1(C78S) allele-replacement strain produced an intermediate number of progeny in the presence of arsenic trioxide relative to the parental N2 and CB4856 strains. However, the CB4856 DBT-1(S78C) allele-replacement strain produced fewer offspring than both parental strains (Figure 3A). Interestingly, the N2 DBT-1(S78) strain had the same level of resistance to arsenic trioxide, as measured by progeny length, as the parental CB4856 strain. However, the CB4856 DBT-1(C78) strain was still more resistant to arsenic trioxide than the parental N2 strain (Figure 3B). These results suggested that additional genetic differences between the N2 and CB4856 strains might interact with the DBT-1(C78S) allele. Nevertheless, these results functionally validate the DBT-1 C78S variant underlies differences in physiological responses in the presence arsenic trioxide.

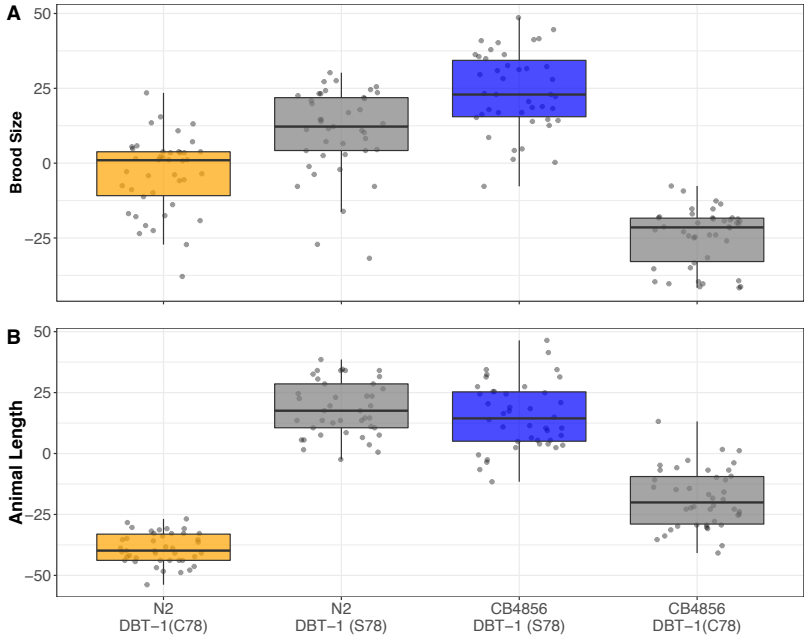

Figure 3: The DBT-1 C78S variant underlies arsenic trioxide sensitivity in *C. elegans.*
Tukey box plots of residual (A) brood size and (B) median animal length after arsenic trioxide exposure are shown (N2, orange; CB4856, blue; allele replacement strains, gray). Labels correspond to the genetic background and the corresponding residue at position 78 of DBT-1 (C for cysteine, S for serine). Every pair-wise strain comparison is significant except for the N2 DBT-1(S78) - CB4856 comparison from animal length (Brood size: Tukey's HSD *p*-value = 1.54E-5; Animal length: *p*-value < 1E-14).

Arsenic trioxide inhibits the DBT-1 C78 allele

Mono-methyl branched chain fatty acids (mmBCFA) are an important class of molecules that are produced via BCAA catabolism (Jia et al. 2016; Kniazeva, Euler, and Han 2008; Kniazeva et al. 2004; Baugh 2013). The production of mmBCFA requires the BCKDH, fatty acid synthase (FASN-1), acetyl-CoA carboxylase (POD-2), fatty acyl elongases (ELO-5/6), β-ketoacyl dehydratase (LET-767), and acyl CoA synthetase (ACS-1) (Watts and Ristow 2017; Entchev et al. 2008; Kniazeva et al. 2004; Kniazeva, Euler, and Han 2008; Jia et al. 2016; Zhu et al. 2013). Strains that lack functional *elo-5*, *elo-6*, or *dbt-1* produce less C15ISO and C17ISO mmBCFAs, arrest at the L1 larval stage, and can be rescued by supplementing the growth media with C15ISO or C17ISO (Jia et al. 2016; Kniazeva, Euler, and Han 2008; Kniazeva et al. 2004) (Figure 4A).

Because DBT-1 is involved in BCAA catabolism, we hypothesized that the DBT-1(C78S)-dependent difference in progeny length between N2 and CB4856 upon arsenic trioxide treatment might be caused by depletion of downstream mmBCFAs. To test this hypothesis, we quantified the abundance of the isomer (ISO) and straight-chain forms of C15 and C17 in the N2, CB4856, and allele-swap genetic backgrounds. We measured the metabolite levels in staged L1 animals and normalized the detected amounts of C15ISO and C17ISO relative to the abundances of straight-chain C15 and C17, respectively, to mitigate confounding effects of differences in developmental speeds that could result from genetic background differences or arsenic trioxide exposure. As expected, we observed a reduction of C15ISO in arsenic-treated animals (Figure 4B). Although C15ISO was more abundant in N2 than in CB4856 animals, arsenic reduced C15ISO production more strongly in N2 than in CB4856, in agreement with our physiological observations that CB4856 was more resistant to arsenic trioxide (Figure 3). The fact that N2 animals had an approximately 1.75-fold higher ISO/straight-chain ratio in mock conditions than CB4856 animals suggested that N2 might require higher levels of mmBCFA and thus be more susceptible to reduction in these fatty acids.

We also quantified C15ISO amounts in the allele-replacement strains N2 DBT-1(S78) and CB4856 DBT-1(C78) when exposed to arsenic (Figure 4B). In both strains, arsenic exposure was correlated with reduced C15ISO production. In agreement with the predicted outcome, N2 DBT1(S78) was less impacted by arsenic than the N2 strain. By contrast, CB4856 DBT-1(C78) was more strongly affected by arsenic than the CB4856 strain. Correspondingly, the observed reduction of C15ISO by arsenic treatment appeared to be greater in CB4856 DBT-1(C78) carrying the N2 allele of DBT-1 (47% decrease; Tukey HSD *p*-value = 0.019) than in N2 DBT-1(S78) (31% decrease; Tukey HSD *p*-value = 0.26). Interestingly, production of C15ISO was significantly increased in CB4856 DBT-1(C78) compared to the parent strain CB4856, whereas C15ISO levels in N2 DBT-1(S78) were not significantly different from those measured for N2. We observed similar trends for the C17ISO/straight-chain ratio (Figure S6) and raw abundances of C15ISO and C17ISO (Figure S7). Notably, we did not detect any significant

differences between the levels of C15 and C17 straight-chain fatty acids, indicating that the effect of the DBT-1 C78S variant was specific to branched-chain fatty acids (Figure S8). These results, in combination with our physiological observations that the C78S allele, explained the majority of the physiological differences between N2 and CB4856 in the presence of arsenic trioxide (Figure 3) and suggested that the DBT-1(C78) allele was inhibited by arsenic trioxide more strongly than DBT-1(S78).

Next, we investigated if mmBCFA supplementation of the growth media used in our physiological assay could rescue the effects of arsenic trioxide toxicity. We exposed the parental and the DBT-1 allele-replacement strains to media containing arsenic trioxide alone, C15ISO alone, or a combination of arsenic trioxide and C15ISO. Median progeny length of arsenic-treated N2 and CB4856 DBT-1(S78C) strains increased by 9% and 15%, respectively, when supplemented with C15ISO (Figure 4C, Figure S9). These C15ISO-derived increases in body length correspond to a 38% and 63% rescue of the allele-specific arsenic affect in the respective genetic backgrounds. By contrast, CB4856 and N2 DBT-1(C78S) median progeny lengths were unaffected by C15ISO supplementation in arsenic trioxide media. Collectively, these data support the hypothesis that the cysteine/serine variant in DBT-1 contributes to arsenic sensitivity in *C. elegans*, and the DBT-1(C78) variant can be partially rescued by supplementation with mmBCFAs.

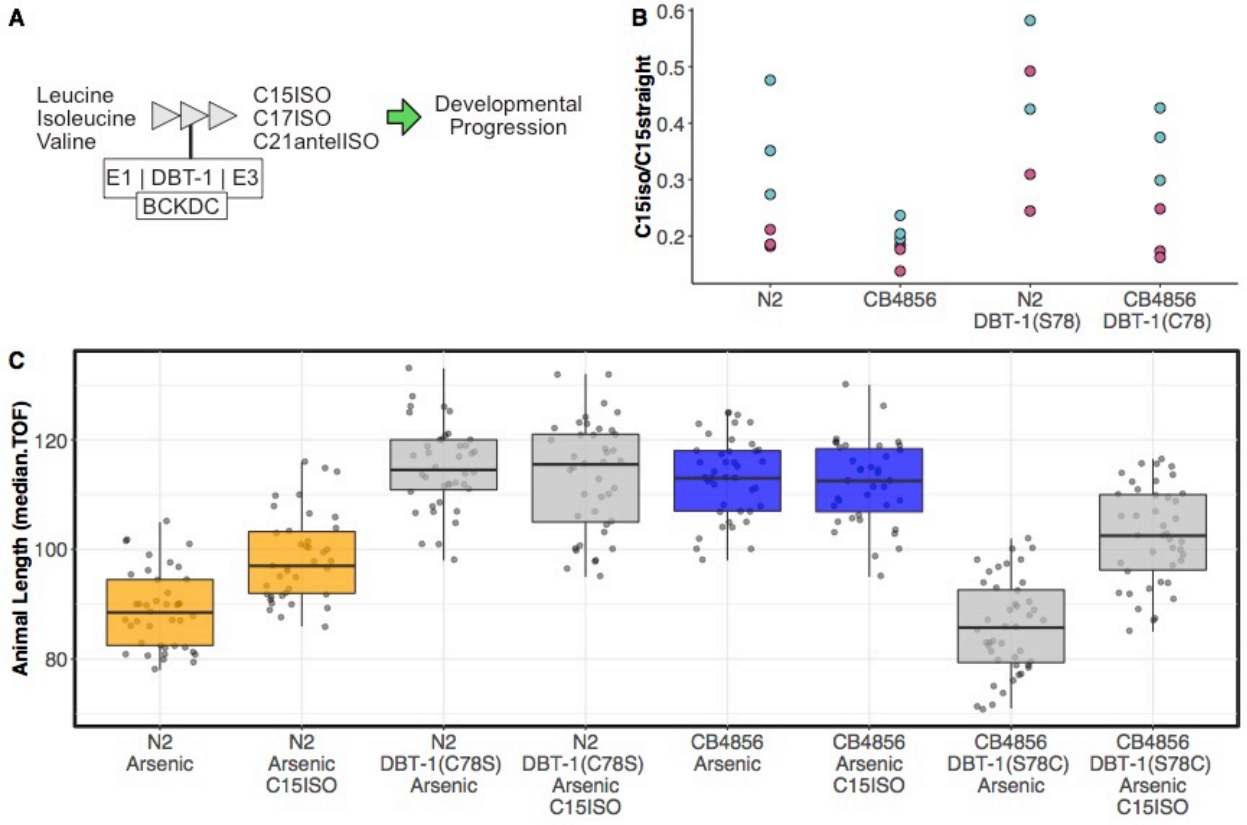

Figure 4: Differential production of mmBCFA underlies DBT-1(C78)-mediated sensitivity to arsenic trioxide.

(A) A simplified model of BCAA catabolism in *C. elegans*. The BCKDH complex, which consists of DBT-1, catalyzes the irreversible oxidative decarboxylation of branched-chain ketoacids. The products of this

breakdown can then serve as building blocks for the mmBCFA that are required for developmental progression. (B) The ratio of C15ISO/C15straight-chain is plotted on the y-axis for three independent replicates of the N2, CB4856, and allele swap strains exposed to control (teal) or 100 µM arsenic trioxide (pink) conditions. The difference between N2 control and N2 arsenic trioxide conditions is statistically significant (Tukey HSD *p*-value = 0.043), but the difference between CB4856 mock and arsenic conditions is not (Tukey HSD *p*-value = 0.075). The difference between N2 swap control and arsenic trioxide conditions is not statistically significant (Tukey HSD *p*-value = 0.26) and the difference between CB4856 swap mock and arsenic conditions is significant (Tukey HSD *p*-value = 0.019). (C) Tukey box plots median animal length after arsenic trioxide or arsenic trioxide and 0.64 µM C15ISO exposure are shown (N2, orange; CB4856, blue; allele replacement strains, gray). Labels correspond to the genetic background and the corresponding residue at position 78 of DBT-1 (C for cysteine, S for serine). Every pair-wise strain comparison is significant except for the N2 DBT-1(S78) - CB4856 comparisons (Tukey's HSD *p*-value < 1.43E-6).

Arsenic exposure increases mmBCFA production and favors a cysteine allele in human DBT1

To test whether our results from *C. elegans* translate to human variation in arsenic sensitivity, we tested the role of DBT1 variation on arsenic trioxide responses and mmBCFA biosynthesis in human cells. The human DBT1 enzyme contains a serine at position 112 that corresponds to the C78 residue in *C. elegans* DBT-1 (Figure 5A). Using CRISPR/Cas9, we edited batch cultures of 293T cells to generate a subset of cells with DBT1(S112C). These cells were exposed to arsenic trioxide or control conditions and we monitored changes in the fraction of cells carrying the DBT1(C112) allele. We found that arsenic exposure caused a 4% increase in the fraction of cells that contained the DBT1(C112) allele (Figure 5B). Though the human DBT1 does not vary within the human population at S112, two residues in close spatial proximity to S112 do vary among individuals in the population (R113C and W84C) (Figure 5A) (Forbes et al. 2008). To test the effects of these residues on arsenic trioxide sensitivity, we performed the same editing and arsenic selection procedure described above. Over the course of the selection experiment, cells with DBT1(W84C) and DBT1(R113C) increased by 2% and 1%, respectively (Figure 5B). All three cysteine edits caused an increase in fitness in batch-edited human cell cultures exposed to arsenic. To determine if branched-chain fatty acid production was altered by arsenic exposure, as we found in *C. elegans*, we measured mmBCFA production in unedited 293T cells in arsenic and mock-treated cultures. We found that overall fatty acid production was markedly reduced in arsenic-treated cultures. In contrast to our observations in *C. elegans*, straight-chain fatty acids were more drastically reduced than ISO fatty acids (Supplemental data 24). These results are consistent with our observations that arsenic does not have as strong of an effect on *C. elegans* strains with the DBT-1 S78 allele. Additionally, the DBT1(C112) allele, similar to the *C. elegans* DBT-1(C78) allele, was associated with higher production of mmBCFAs.

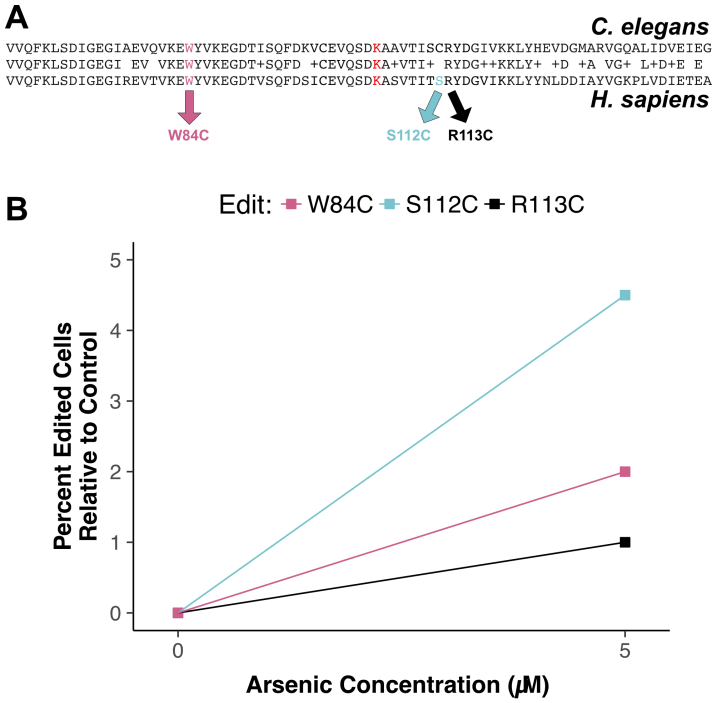

Figure 5: Protective effect of cysteine residues in human DBT1.
A) Alignment of *C. elegans* DBT-1 and *H. sapiens* DBT1. The residues tested for an arsenic-specific effect are indicated with arrows - W84C (pink), S112C (blue), and R113C (black). The lysine that is post-translationally modified with a lipoid acid is highlighted in red. B) The fraction of human cells that contain the W84C, S112C, or R113C amino acid change in DBT1 in the presence of 0 or 5 μM arsenic trioxide are shown. The fraction of edited cells is normalized to the fraction edited in the 0 μM arsenic condition. Each dot corresponds to the mean of two replicate experiments.

Discussion

In this study, we characterized the effects of *C. elegans* natural genetic variation on physiological responses to the pervasive environmental toxin arsenic trioxide. Though the effects of this toxin have been extensively studied in a variety of systems (Bergquist et al. 2009; Ratnaike 2003; Mandal and Suzuki 2002; Paul et al. 2014; Shen et al. 2013), recent evidence from human population studies have revealed local adaptations within region-specific subpopulations (Schlebusch et al. 2015; Fujihara et al. 2009; Gomez-Rubio et al. 2010; Li et al. 2017). Our investigation into the natural variation in *C. elegans* responses to arsenic trioxide led to the discovery of a novel mechanism by which this compound could elicit toxicity. We show that arsenic trioxide differentially inhibits two natural alleles of the E2 domain of the BCKDH complex, which is encoded by the *dbt-1* gene. Specifically, strains with the DBT-1(C78) allele are more sensitive to arsenic trioxide than strains carrying the DBT-1(S78) allele, as measured by progeny production and growth (Figure 3). Furthermore, we show that the increased sensitivity of the DBT-1(C78) allele is largely explained by differences in the production of mmBCFAs (Figure 4B-C), which are critical molecules for developmental progression beyond the first larval stage. Arsenic is thought to inhibit the activity of both the pyruvate dehydrogenase

(PDH) and the α-ketoglutarate (KGDH) dehydrogenase complexes through interactions with the reduced form of lipoate (Bergquist et al. 2009), which is the cofactor for the E2 domain of these complexes. Like the PDH and KGDH complexes, the E2 domain of BCKDH complex requires the cofactor lipoate to perform its enzymatic function (Pettit, Yeaman, and Reed 1978; Heffelfinger, Sewell, and Danner 1983; Yeaman 1989). The inhibition of DBT-1 by arsenic trioxide could involve three-point coordination of arsenic by the C78 thiol and the reduced thiol groups of the nearby lipoate. However, based on the crystal structure (PDB:1Y8N), the atomic distance between the C78 thiol group and the thiol groups from the lipoylated lysine is ~32 Å, which might be too large a distance for coordinating arsenic (Kato et al. 2005) (Figure S10). Alternatively, arsenic trioxide could inhibit DBT-1(C78) through coordination between the thiol groups of C78 and C65 (~8.5 Å) (Figure S10). Analogous thiol-dependent mechanisms have been proposed for the inhibition of other enzymes by arsenic (Shen et al. 2013). Despite structural similarities and a shared cofactor, no evidence in the literature indicates that BCKDH is inhibited by arsenic trioxide, so these results demonstrate the first connection of arsenic toxicity to BCKDH E2 subunit inhibition.

Multiple sequence alignments show that cysteine residues C65 and C78 of *C. elegans* DBT-1 correspond to residues S112 and C99 of human DBT1 (Figure 5A). Though DBT1 does not vary at position 112 within the human population, two residues (R113C and W84C) in close spatial proximity do (Forbes et al. 2008). We hypothesized that cysteine variants in DBT1 would sensitize human cells to arsenic trioxide. Interestingly, we found that the cysteine variants (W84C, S112C, and R113C) proliferated more rapidly than the parental cells in the presence of arsenic. In agreement with these results, a growing body of evidence suggests that certain cancer cells upregulate components involved in BCAA, and this upregulation promotes tumor growth (Burrage et al. 2014; Tönjes et al. 2013). Perhaps the increased proliferation of human cell lines that contain the DBT1 C112 allele (Figure 5) is caused by increased activity of the BCKDH complex. In agreement, we found that *C. elegans* strains with the DBT-1 C78 allele produce more mmBCFAs than strains with the S78 allele (Figure 4b and Figure S6). It is worth noting that human cell lines grown in culture do not have the same strict requirements for mmBCFA, and the requirements for different fatty acids are variable among diverse immortalized cell lines (Hughes-Fulford, Chen, and Tjandrawinata 2001; Agostini et al. 2004). Furthermore, in *C. elegans*, the developmental defects associated with *dbt-1* loss-of-function can be rescued by neuronal-specific expression of *dbt-1* (Jia et al. 2016), suggesting that the physiological requirements of mmBCFA in *C. elegans* depend on the coordination of multiple tissues that cannot be recapitulated with cell-culture experiments. These results further highlight the complexity of arsenic toxicity as well as the physiological requirements of BCAA within and across species and could explain the discrepancy between the physiological effects we observed in *C. elegans* and human cell-line experiments. Given that arsenic trioxide has become the standard-of-care for treating AML (Coombs, Tavakkoli, and Tallman 2015) and is gaining traction in treating other leukemias, our results indicate that further exploration of the effects of arsenic and BCAA catabolism on cancer growth is essential.

The C78 allele of DBT-1 is likely the derived allele in the *C. elegans* population because all other organisms have a serine at the corresponding position. The loss of the serine allele in the *C. elegans* population might have been caused by relaxed selection at this locus. It is hypothesized that the *C. elegans* species originated from the Pacific Rim and that the ancestral

state more closely resembles the CB5846 strain than the N2 strain (Andersen et al. 2012; Thompson et al. 2015). The CB4856 strain was isolated from the Hawaiian island of O'ahu (Hodgkin and Doniach 1997). The Hawaiian islands have elevated levels of arsenic in the soil from volcanic activity, the farming of cane sugar, former construction material (canec) production facilities, or wood treatment plants (Hawaii.gov). It is possible that as the *C. elegans* species spread across the globe into areas with lower levels of arsenic in the soil and water, the selective pressure to maintain high arsenic tolerance was relaxed and the cysteine allele appeared. Alternatively, higher mmBCFA levels in strains with the DBT-1(C78) allele (Figure S7) might cause faster development in certain conditions, although we did not observe allele-specific growth differences in laboratory conditions. Despite these clues suggesting selection in local environments, the genomic region surrounding the *dbt-1* locus does not appear to have a strong signature of selection as measured by Tajima's D (Tajima 1989) (Figure S11), and the strains with the DBT-1 S78 allele show no signs of geographic clustering (Figure S12). In the future, it will be important to sample additional *C. elegans* wild strains and measure arsenic levels in the natural substrates to further explore this possible connection. Our study suggests that *C. elegans* is a powerful model to investigate the molecular mechanisms for how populations respond to environmental toxins.

Materials and methods

Strains

Animals were fed the bacterial strain OP50 and grown at 20°C on modified nematode growth medium (NGM), containing 1% agar and 0.7% agarose to prevent burrowing of the wild isolates (Boyd, Smith, and Freedman 2012). For each assay, strains were grown for five generations with no strain entering starvation or encountering dauer-inducing conditions (Andersen et al. 2014). Wild *C. elegans* isolates used for genome-wide association and recombinant inbred advanced intercross lines (RIAILs) used for linkage mapping have been described previously (Cook, Zdraljevic, Tanny, et al. 2016; Cook, Zdraljevic, Roberts, et al. 2016; Andersen et al. 2015). Strains constructed for this manuscript are listed in Supplemental table 1.

High-throughput fitness assay

We used the high-throughput fitness assay (HTA) described previously (Andersen et al. 2015). In short, strains are passaged for four generations before bleach-synchronization and aliquoted to 96-well microtiter plates at approximately one embryo per microliter in K medium (Boyd, Smith, and Freedman 2012). The final concentration of NaCl in the K medium for the genome-wide association (GWA) and linkage mapping assays was 51 mM. For all subsequent experiments the final NaCl concentration was 10.2 mM. The following day, hatched and synchronized L1 animals were fed HB101 bacterial lysate (Pennsylvania State University Shared Fermentation Facility, State College, PA, (García-González et al. 2017)) at a final concentration of 5 mg/ml and grown for two days at 20ºC. Next, three L4 larvae were sorted using a large-particle flow cytometer (COPAS BIOSORT, Union Biometrica, Holliston, MA) into microtiter plates that contain HB101 lysate at 10 mg/ml, K medium, 31.25 µM kanamycin, and either drug dissolved in 1% water or 1% water alone. The animals were then grown for four

days at 20ºC. The resulting populations were treated with sodium azide (50 mM) prior to being measured with the BIOSORT.

Calculation of fitness traits for genetic mappings

Phenotype data generated using the BIOSORT were processed using the R package *easysorter*, which was specifically developed for processing this type of data (Shimko and Andersen 2014). Briefly, the function *read_data*, reads in raw phenotype data and runs a support vector machine to identify and eliminate bubbles. Next, the *remove_contamination* function eliminates any wells that were identified as contaminated prior to scoring population parameters. The *sumplate* function is then used to generate summary statistics of the measured parameters for each animal in each well. These summary statistics include the 10th, 25th, 50th, 75th, and 90th quantiles for time of flight (TOF), which corresponds to animal length. Measured brood sizes (n) are normalized by the number of animals that were originally sorted into each well (norm.n). After summary statistics for each well are calculated, we accounted for differences between assays using the the *regress(assay=TRUE)* function in the *easysorter* package. Outliers in the GWA and linkage mapping experiments were identified and eliminated using the *bamf_prune* function in *easysorter*. For follow-up experiments that contained multiple replicates for each strain, we eliminated strain replicates that were more than two standard deviations from the strain mean for each condition tested. Finally, drug-specific effects were calculated using the *regress(assay=FALSE)* function from *easysorter*, which accounts for strain-specific differences in growth parameters present in control conditions.

Arsenic trioxide dose-response assays

All dose-response experiments were performed on four genetically diverged strains (N2, CB4856, DL238, and JU258) in technical quadruplicates prior to performing GWA and linkage mapping experiments (Supplemental data 1). Animals were assayed using the HTA, and phenotypic analyses were performed as described above. The arsenic trioxide concentration for GWA and linkage mapping experiments was chosen based on an observable effect for animal length and brood size phenotypes in the presence of arsenic.

Linkage mapping

A total of 262 RIAILs were phenotyped in the HTA described previously for control and arsenic trioxide conditions (Andersen et al. 2015; Zdraljevic et al. 2017). The phenotype and genotype data were entered into R and scaled to have a mean of zero and a variance of one for linkage analysis (Supplemental data 2-4). Quantitative trait loci (QTL) were detected by calculating logarithm of odds (LOD) scores for each marker and each trait as $-n(ln(1-r^2)/2ln(10))$, where r is the Pearson correlation coefficient between RIAIL genotypes at the marker and phenotype trait values (Bloom et al. 2013). The maximum LOD score for each chromosome for each trait was retained from three iterations of linkage mappings (Supplemental data 5). We randomly permuted the phenotype values of each RIAIL while maintaining correlation structure among phenotypes 1000 times to estimate the significance threshold empirically. The significance threshold was set using a genome-wide error rate of 5%. Confidence intervals were defined as the regions contained within a 1.5 LOD drop from the maximum LOD score (Broman et al. 2003).

Near-isogenic line (NIL) generation

NILs were generated by crossing N2xCB4856 RIAILs to each parental genotype. For each NIL, eight crosses were performed followed by six generations of selfing to homozygose the genome. Reagents used to generate NILs are detailed in Supplemental table 1 and 2. The NILs responses to 1000 µM arsenic trioxide were quantified using the HTA described above (Supplemental data 6-8). NIL whole-genome sequencing and analysis was performed as described previously (Brady et al. 2018) (Supplemental data 9).

Genome-wide association mapping

Genome-wide association (GWA) mapping was performed using phenotype data from 86 *C. elegans* isotypes (Supplemental data 10-13). We used the *cegwas* R package for association mapping and post-mapping processing (Cook, Zdraljevic, Roberts, et al. 2016). This package uses the EMMA algorithm for performing association mapping and correcting for population structure (Kang et al. 2008), which is implemented by the *GWAS* function in the *rrBLUP* package (Endelman 2011). Specifically, the *GWAS* function in the *rrBLUP* package was called with the following command: *rrBLUP::GWAS(pheno = ph, geno = y, K = kin, min.MAF = 0.05, n.core = 1, P3D = FALSE, plot = FALSE)*. The kinship matrix used for association mapping was generated using a whole-genome high-quality single-nucleotide variant (SNV) set from CeNDR release 20160408 (Cook, Zdraljevic, Tanny, et al. 2016; Zdraljevic et al. 2017; Evans et al. 2017) and the *A.mat* function from the *rrBLUP* package. SNVs previously identified using RAD-seq (Andersen et al. 2012) that had at least 5% minor allele frequency in the 86 isotype set were used for performing GWA mappings. Association mappings that contained at least one SNV that had a value greater than the Bonferroni-corrected value were processed further using fine mapping. Brood size and animal length significance scores can be found in Supplemental data 14.

Principal component analysis

The COPAS BIOSORT quantifies individual animal length (TOF), optical density (EXT), fluorescence (green, yellow, and red), and total animals in a well normalized by the number of animals initially sorted into the well (brood size). All of these measurements were then summarized using the *easysorter* package to generate various summary statistics of each raw BIOSORT parameter, including five distribution quantiles and measures of dispersion (Andersen et al. 2015). Prior to principal component analysis (PCA), HTA phenotypes were scaled to have a mean of zero and a standard deviation of one using the *scale* function in R. PCA was performed using the *prcomp* function in R (Team 2017) (Supplemental data 15). The variance explained for each principal components is located in Supplemental data 16. Genome-wide mapping results using the first principal component are available in Supplemental data 17.

Fine mapping

We previously described the identification of QTL confidence intervals and fine-mapping (Zdraljevic et al. 2017). In short, we used the *process_correlations()* and the *variant_correlation()* functions in the *cegwas* package. These functions calculate the *p*-value associated with the Spearman's correlation coefficient between each variant in the QTL

591 confidence interval and the kinship-corrected phenotype used in the GWA (Supplemental data
592 18).
593
594 **Generation of *dbt-1* allele replacement strains**
595 Allele replacement strains were generated using CRISPR/Cas9-mediated genome editing, using
596 the co-CRISPR approach (Kim et al. 2014) with Cas9 ribonucleoprotein delivery (Paix et al.
597 2015). Alt-R™ crRNA and tracrRNA (Supplemental table 2) were purchased from IDT (Skokie,
598 IL). tracrRNA (IDT, 1072532) was injected at a concentration of 13.6 µM. The *dpy-10* and the
599 *dbt-1* crRNAs were injected at 4 µM and 9.6 µM, respectively. The *dpy-10* and the *dbt-1* single-
600 stranded oligodeoxynucleotides (ssODN) repair templates were injected at 1.34 µM and 4 µM,
601 respectively. Cas9 protein (IDT, 1074182) was injected at 23 µM. To generate injection mixes,
602 the tracrRNA and crRNAs were incubated at 95ºC for five minutes and 10ºC for 10 minutes.
603 Next, Cas9 protein was added and incubated for five minutes at room temperature. Finally,
604 repair templates and nuclease-free water were added to the mixtures and loaded into pulled
605 injection needles (1B100F-4, World Precision Instruments, Sarasota, FL). Individual injected P_0
606 animals were transferred to new 6 cm NGM plates approximately 18 hours after injections.
607 Individual F_1 rollers were then transferred to new 6 cm plates to generate self-progeny. The
608 region surrounding the desired S78C (or C78S) edit was then amplified from F_1 rollers using
609 primers oECA1163 and oECA1165. The PCR products were digested using the *Sfc*I restriction
610 enzyme (R0561S, New England Biolabs, Ipswich, MA). Differential band patterns signified
611 successfully edited strains because the N2 S78C, which is encoded by the CAG codon, creates
612 an additional *Sfc*I cut site. Non-Dpy, non-Rol progeny from homozygous edited F_1 animals were
613 propagated. If no homozygous edits were obtained, heterozygous F_1 progeny were propagated
614 and screened for the presence of the homozygous edits. F_1 and F_2 progeny were then Sanger
615 sequenced to verify the presence of the proper edited sequence. The phenotypes of allele swap
616 strains in control and arsenic trioxide conditions were measured using the HTA described above
617 (Supplemental data 6-8). PCA phenotypes for allele-swap strains were generated the same way
618 as described above for GWA mapping traits and are located in Supplemental data 19.
619
620 **Rescue with 13-methyltetradecanoic acid**
621 Strains were grown as described for a standard HTA experiment. In addition to adding arsenic
622 trioixde to experimental wells, we also added a range of C15iso (13-methyltetradecanoic acid,
623 Matreya Catalog # 1605) concentrations to assay rescue of arsenic effects (Supplemental data
624 20-21).
625
626 **Growth conditions for metabolite profiling**
627 Chunks (~1 cm) were taken from starved plates and placed on multiple fresh 10 cm plates. Prior
628 to starvation, animals were washed off of the plates using M9, and embryos were prepared by
629 bleach-synchronization. Approximately 40,000 embryos were resuspended in 25 ml of K
630 medium and allowed to hatch overnight at 20ºC. L1 larvae were fed 15 mg/ml of HB101 lysate
631 the following morning and allowed to grow at 20ºC for 72 hours. We harvested 100,000
632 embryos from gravid adults by bleaching. These embryos were hatched overnight in 50 ml of K
633 medium in a 125 ml flask. The following day, we added arsenic trioxide to a final concentration
634 of 100 µM and incubated the cultures for 24 hours. After 24 hours, we added HB101 bacterial

lysate (2 mg/ml final) to each culture. Finally, we transferred the cultures to 50 ml conical tubes, centrifuged the cultures at 3000 RPM for three minutes, and separated the pellet and supernatant. The supernatant and pellets from the cultures were frozen at -80ºC and prepared for analysis.

Nematode extraction

Pellets were lyophilized 18-24 hours using a VirTis BenchTop 4K Freeze Dryer until a chalky consistency was achieved. Dried pellets were transferred to 1.5 mL microfuge tubes and dry pellet weight recorded. Pellets were disrupted in a Spex 1600 MiniG tissue grinder after the addition of three stainless steel grinding balls to each sample. Microfuge tubes were placed in a Cryoblock (Model 1660) cooled in liquid nitrogen, and samples were disrupted at 1100 RPM for two cycles of 30 seconds. At this point, each sample was individually dragged across a microfuge tube rack eight times, inverted, and flicked five times to prevent clumping. This process was repeated two additional rounds for a total of six disruptions. Pellets were transferred to 4 mL glass vials in 3 mL 100% ethanol. Samples were sonicated for 20 minutes (on/off pulse cycles of two seconds at power 90 A) using a Qsonica Ultrasonic Processor (Model Q700) with a water bath cup horn adaptor (Model 431C2). Following sonication, glass vials were centrifuged at 2750 RCF for five minutes in an Eppendorf 5702 Centrifuge using rotor F-35-30-17. The resulting supernatant was transferred to a clean 4 mL glass vial and concentrated to dryness in an SC250EXP Speedvac Concentrator coupled to an RVT5105 Refrigerated Vapor Trap (Thermo Scientific). The resulting powder was suspended in 100% ethanol according to its original dry pellet weight: 0.01 mL 100% ethanol per mg of material. The suspension was sonicated for 10 minutes (pulse cycles of two seconds on and three seconds off at power 90 A) followed by centrifugation at 20,817 RCF in a refrigerated Eppendorf centrifuge 5417R at 4°C. The resulting supernatant was transferred to an HPLC vial containing a Phenomenex insert (cat #AR0-4521-12) and centrifuged at 2750 RCF for five minutes in an Eppendorf 5702 centrifuge. The resulting supernatant was transferred to a clean HPLC vial insert and stored at -20°C or analyzed immediately.

Mass spectrometric analysis

Reversed-phase chromatography was performed using a Dionex Ultimate 3000 Series LC system (HPG-3400 RS High Pressure pump, TCC-3000RS column compartment, WPS-3000TRS autosampler, DAD-3000 Diode Array Detector) controlled by Chromeleon Software (ThermoFisher Scientific) and coupled to an Orbitrap Q-Exactive mass spectrometer controlled by Xcalibur software (ThermoFisher Scientific). Metabolites were separated on a Kinetex EVO C18 column, 150 mm x 2.1 mm, particle size 1.7 µm, maintained at 40°C with a flow rate of 0.5 mL/min. Solvent A: 0.1% ammonium acetate in water; solvent B: acetonitrile (ACN). A/B gradient started at 5% B for 30 seconds, followed by a linear gradient to 95% B over 13.5 minutes, then a linear gradient to 100% B over three minutes. 100% B was maintained for one minute. Column was washed after each run with 5:1 isopropanol:ACN, flow rate of 0.12 mL/min for five minutes, followed by 100% ACN for 2.9 minutes, a linear gradient to 95:5 water:ACN over 0.1 minutes, and then 95:5 water:ACN for two minutes with a flow rate of 0.5 mL/min. A heated electrospray ionization source (HESI-II) was used for the ionization with the following mass spectrometer parameters: spray voltage: 3 kV; capillary temperature: 320°C; probe heater

temperature: 300°C; sheath gas: 70 AU; auxiliary gas flow: 2 AU; resolution: 240,000 FWHM at m/z 200; AGC target: 5e6; maximum injection time: 300 ms. Each sample was analyzed in negative and positive modes with m/z range 200-800. Fatty acids and most ascarosides were detected as $[M-H]^-$ ions in negative ionization mode. Peaks of known abundant ascarosides and fatty acids were used to monitor mass accuracy, chromatographic peak shape, and instrument sensitivity for each sample. Processed metabolite measures can be found in Supplemental data 22.

Statistical analyses

All *p*-values testing the differences of strain phenotypes in the NIL, allele-replacement, and C15ISO experiments were performed in R using the *TukeyHSD* function with an ANOVA model with the formula (*phenotype* ~ *strain*). *p*-values of individual pairwise strain comparisons are reported in each figure legend.

CRISPR-Cas9 gene editing in human cells

Gene-editing experiments were performed in a single parallel culture experiment using human 293T cells (ATCC) grown in DMEM with 10% FBS. On day zero, 300,000 cells were seeded per well in a six-well plate format. The following day, two master mixes were prepared: a) LT-1 transfection reagent (Mirus) was diluted 1:10 in Opti-MEM and incubated for five minutes; b) a DNA mix of 500 ng Cas9-sgRNA plasmid with 250 pmol repair template oligonucleotide (Supplemental table 2) was diluted in Opti-MEM in a final volume of 100 µL. 250 µL of the lipid mix was added to each of the DNA mixes and incubated at room temperature for 25 minutes. Following incubation, the full 350 µL volume of DNA and lipid mix was added dropwise to the cells. These six-well plates were then centrifuged at 1000 x g for 30 minutes. After six hours, the media on the cells was replaced. For the next six days, cells were expanded and passaged as needed. On day seven, one million cells were taken from each set of edited and unedited cells and placed into separate T75s with either media-only or 5 µM arsenic-containing media. Days seven to fourteen, arsenic and media-only conditions were maintained at healthy cell densities. Days fourteen to eighteen, arsenic exposed cell populations were maintained off arsenic to allow the populations to recover prior to sequencing. Media-only conditions were maintained in parallel. On day eighteen, all arsenic and media-only conditions were pelleted for genomic DNA extraction.

Analysis of CRISPR-Cas9 editing in human cells

Genomic DNA was extracted from cell pellets using the QIAGEN (QIAGEN, Hilden, Germany) Midi or Mini Kits based on the size of the cell pellet (51183, 51104) according to the manufacturer's recommendations. DBT1 loci were first amplified with 17 cycles of PCR using a touchdown protocol and the NEBnext 2x master mix (New England Biolabs M0541). The resulting product served as input to a second PCR, using primers that appended a sample-specific barcode and the necessary adaptors for Illumina sequencing. The resulting DNA was pooled, purified with SPRI beads (A63880, Beckman Coulter, Brea, CA), and sequenced on an Illumina MiSeq with a 300-nucleotide single-end read with an eight nucleotide index read. For each sample, the number of reads exactly matching the wild-type and edited DBT1 sequence were determined (Supplemental data 23)

Preparing human cells for Mass Spectroscopy

Mass spectroscopy experiments used human 293T cells (ATCC) grown in DMEM with 10% FBS. On day zero, 150,000 cells were seeded into 15 cm tissue cultures dishes with 15 mL of either 2.5 μM arsenic or no arsenic media. Each condition had five replicates. On day three, the no arsenic cells were approaching confluence and required passaging. Arsenic conditions were at ~30% confluence and received a media change. On day seven, both conditions were near confluence, media was removed, and plates were rinsed with ice cold PBS, remaining liquid removed. Plates were frozen at -80ºC before processing for mass spectrometric analysis. Metabolite measurements can be found in Supplemental data 24.

Tajima's D calculation

We used the VCF corresponding to CeNDR release 20160408 (Supplemental data 25a-b) to calculate Tajima's D. Tajima's D was calculated using the *tajimas_d* function in the *cegwas* package using default parameters (window size = 500 SNVs, sliding window distance = 50 SNVs, outgroup = N2) (Supplemental data 26). Isolation locations of strains can be found in Supplemental data 27.

Author Contributions:

SZ and ECA conceptualized and designed the *C. elegans* experiments. CS and JGD designed the human cell-line experiments. SZ performed *C. elegans* experiments. TAC helped with preparation of *C. elegans* for metabolite extraction. CS performed the human cell-line experiments. BWF processed *C. elegans* samples for metabolite extraction and performed and analyzed the metabolite profiling experiments. OP and FJT prepared and analyzed metabolite experiments during initial optimization of the growth conditions. SCB helped construct an allele-replacement strain. Formal data curation and analysis of *C. elegans* experiments, excluding metabolite profiling, was performed by SZ. SZ wrote the manuscript and processed and analyzed the data for the manuscript figures. All authors contributed to the editing of the manuscript. Supervision of the project was performed by ECA, FCS, and JGD.

Funding:

This work was supported by a National Institutes of Health R01 subcontract to ECA (GM107227), the Chicago Biomedical Consortium with support from the Searle Funds at the Chicago Community Trust, a Sherman-Fairchild Cancer Innovation Award to ECA, and an American Cancer Society Research Scholar Grant to ECA (127313-RSG-15-135-01-DD), along with support from the Cell and Molecular Basis of Disease training grant (T32GM008061) to SZ. JGD is a Merkin Institute Fellow and is supported by the Next Generation Fund at the Broad Institute of MIT and Harvard. FCS, BWF, OP, and FJT were supported by R01 GM088290. The funders had no role in study design, data collection and analysis, decision to publish, or preparation of the manuscript.

Acknowledgments:

The authors would like to thank Samuel Rosenberg for assistance on early mappings of drug sensitivities, Mudra Hegde of the Broad Institute for assistance with sequence analysis, and members of the Andersen laboratory for critical reading of this manuscript.

References

Adeva-Andany, María M., Laura López-Maside, Cristóbal Donapetry-García, Carlos Fernández-Fernández, and Cristina Sixto-Leal. 2017. "Enzymes Involved in Branched-Chain Amino Acid Metabolism in Humans." *Amino Acids* 49 (6): 1005–28. https://doi.org/10.1007/s00726-017-2412-7.

Agostini, Michelle, Sabrina D. Silva, Karina G. Zecchin, Ricardo D. Coletta, Jacks Jorge, Massimo Loda, and Edgard Graner. 2004. "Fatty Acid Synthase Is Required for the Proliferation of Human Oral Squamous Carcinoma Cells." *Oral Oncology* 40 (7): 728–35. https://doi.org/10.1016/j.oraloncology.2004.01.011.

Andersen, Erik C., Joshua S. Bloom, Justin P. Gerke, and Leonid Kruglyak. 2014. "A Variant in the Neuropeptide Receptor Npr-1 Is a Major Determinant of *Caenorhabditis Elegans* Growth and Physiology." 10 (2): e1004156. https://doi.org/10.1371/journal.pgen.1004156.

Andersen, Erik C., Joshua S. Bloom, Leonid Kruglyak, Marie-Anne Félix, Rajarshi Ghosh, Justin P. Gerke, Joshua A. Shapiro, and Jonathan R. Crissman. 2012. "Chromosome-Scale Selective Sweeps Shape *Caenorhabditis Elegans* Genomic Diversity." *Nature Genetics* 44 (3): 285–90. https://doi.org/10.1038/ng.1050.

Andersen, Erik C., Tyler C. Shimko, Jonathan R. Crissman, Rajarshi Ghosh, Joshua S. Bloom, Hannah S. Seidel, Justin P. Gerke, and Leonid Kruglyak. 2015. "A Powerful New Quantitative Genetics Platform, Combining *Caenorhabditis Elegans* High-Throughput Fitness Assays with a Large Collection of Recombinant Strains." *G3* 5 (5): g3.115.017178–920. https://doi.org/10.1534/g3.115.017178.

Antman, K. H. 2001. "Introduction: The History of Arsenic Trioxide in Cancer Therapy." *The Oncologist* 6 Suppl 2: 1–2. https://doi.org/10.1634/theoncologist.6-suppl_2-1.

Baugh, L. R. 2013. "To Grow or Not to Grow: Nutritional Control of Development During Caenorhabditis Elegans L1 Arrest." *Genetics* 194 (3): 539–55. https://doi.org/10.1534/genetics.113.150847.

Bergquist, Erik R., Robert J. Fischer, Kent D. Sugden, and Brooke D. Martin. 2009. "Inhibition by Methylated Organo-Arsenicals of the Respiratory 2-Oxo-Acid Dehydrogenases." *Journal of Organometallic Chemistry* 694 (6): 973–80. https://doi.org/10.1016/j.jorganchem.2008.12.028.

Bloom, Joshua S., Ian M. Ehrenreich, Wesley T. Loo, Thúy-Lan Võ Lite, and Leonid Kruglyak. 2013. "Finding the Sources of Missing Heritability in a Yeast Cross." *Nature* 494 (7436): 1–6. https://doi.org/10.1038/nature11867.

Boyd, Windy A., Marjolein V. Smith, and Jonathan H. Freedman. 2012. "Caenorhabditis Elegans as a Model in Developmental Toxicology." *Methods in Molecular Biology* 889 (Chapter 3): 15–24. https://doi.org/10.1007/978-1-61779-867-2_3.

Brady, Shannon, Kathryn Evans, Joshua Bloom, Robyn Tanny, Daniel Cook, Sarah Giuliani, Stephen Hippleheuser, Mostafa Zamanian, and Erik Andersen. 2018. "Common Loci Underlie Natural Variation in Diverse Toxin Responses." *bioRxiv*. https://doi.org/10.1101/325399.

Broman, Karl W., Hao Wu, Saunak Sen, and Gary A. Churchill. 2003. "R/qtl: QTL Mapping in Experimental Crosses." *Bioinformatics* 19 (7): 889–90. http://eutils.ncbi.nlm.nih.gov/entrez/eutils/elink.fcgi?dbfrom=pubmed&id=12724300&retmode=ref&cmd=prlinks.

Burrage, Lindsay C., Sandesh C. S. Nagamani, Philippe M. Campeau, and Brendan H. Lee. 2014. "Branched-Chain Amino Acid Metabolism: From Rare Mendelian Diseases to More Common Disorders." *Human Molecular Genetics* 23 (R1): R1–8. https://doi.org/10.1093/hmg/ddu123.

Chen, G. Q., X. G. Shi, W. Tang, S. M. Xiong, J. Zhu, X. Cai, Z. G. Han, et al. 1997. "Use of Arsenic Trioxide (As2O3) in the Treatment of Acute Promyelocytic Leukemia (APL): I.

As2O3 Exerts Dose-Dependent Dual Effects on APL Cells." *Blood* 89 (9): 3345–53. https://www.ncbi.nlm.nih.gov/pubmed/9129041.

Chung, Chi-Jung, Yu-Mei Hsueh, Chyi-Huey Bai, Yung-Kai Huang, Ya-Li Huang, Mo-Hsiung Yang, and Chien-Jen Chen. 2009. "Polymorphisms in Arsenic Metabolism Genes, Urinary Arsenic Methylation Profile and Cancer." *Cancer Causes & Control: CCC* 20 (9): 1653–61. https://doi.org/10.1007/s10552-009-9413-0.

Cook, Daniel E., Stefan Zdraljevic, Joshua P. Roberts, and Erik C. Andersen. 2016. "CeNDR, the Caenorhabditis Elegans Natural Diversity Resource." *Nucleic Acids Research*, October. https://doi.org/10.1093/nar/gkw893.

Cook, Daniel E., Stefan Zdraljevic, Robyn E. Tanny, Beomseok Seo, David D. Riccardi, Luke M. Noble, Matthew V. Rockman, et al. 2016. "The Genetic Basis of Natural Variation in Caenorhabditis Elegans Telomere Length." *Genetics* 204 (1): 371–83. https://doi.org/10.1534/genetics.116.191148.

Coombs, C. C., M. Tavakkoli, and M. S. Tallman. 2015. "Acute Promyelocytic Leukemia: Where Did We Start, Where Are We Now, and the Future." *Blood Cancer Journal* 5 (April): e304. https://doi.org/10.1038/bcj.2015.25.

Emi, Nobuhiko. 2017. "Arsenic Trioxide: Clinical Pharmacology and Therapeutic Results." In *Chemotherapy for Leukemia*, 221–38. Springer, Singapore. https://doi.org/10.1007/978-981-10-3332-2_13.

Endelman, Jeffrey B. 2011. "Ridge Regression and Other Kernels for Genomic Selection with R Package rrBLUP." *The Plant Genome Journal* 4 (3): 250–56. https://doi.org/10.3835/plantgenome2011.08.0024.

Entchev, Eugeni V., Dominik Schwudke, Vyacheslav Zagoriy, Vitali Matyash, Aliona Bogdanova, Bianca Habermann, Lin Zhu, Andrej Shevchenko, and Teymuras V. Kurzchalia. 2008. "LET-767 Is Required for the Production of Branched Chain and Long Chain Fatty Acids in Caenorhabditis Elegans." *The Journal of Biological Chemistry* 283 (25): 17550–60. https://doi.org/10.1074/jbc.M800965200.

Evans, Kathryn S., Yuehui Zhao, Shannon C. Brady, Lijiang Long, Patrick T. McGrath, and Erik C. Andersen. 2017. "Correlations of Genotype with Climate Parameters Suggest Caenorhabditis Elegans Niche Adaptations." *G3* 7 (1): 289–98. https://doi.org/10.1534/g3.116.035162.

Forbes, S. A., G. Bhamra, S. Bamford, E. Dawson, C. Kok, J. Clements, A. Menzies, J. W. Teague, P. A. Futreal, and M. R. Stratton. 2008. "The Catalogue of Somatic Mutations in Cancer (COSMIC)." *Current Protocols in Human Genetics / Editorial Board, Jonathan L. Haines ... [et Al.]* Chapter 10 (April): Unit 10.11. https://doi.org/10.1002/0471142905.hg1011s57.

Fujihara, Junko, Yoshimi Fujii, Tetsuro Agusa, Takashi Kunito, Toshihiro Yasuda, Tamami Moritani, and Haruo Takeshita. 2009. "Ethnic Differences in Five Intronic Polymorphisms Associated with Arsenic Metabolism within Human Arsenic (+3 Oxidation State) Methyltransferase (AS3MT) Gene." *Toxicology and Applied Pharmacology* 234 (1): 41–46. https://doi.org/10.1016/j.taap.2008.09.026.

García-González, Aurian P., Ashlyn D. Ritter, Shaleen Shrestha, Erik C. Andersen, L. Safak Yilmaz, and Albertha J. M. Walhout. 2017. "Bacterial Metabolism Affects the C. elegans Response to Cancer Chemotherapeutics." *Cell* 169 (3): 431–41.e8. https://doi.org/10.1016/j.cell.2017.03.046.

Gomez-Rubio, Paulina, Maria M. Meza-Montenegro, Ernesto Cantu-Soto, and Walter T. Klimecki. 2010. "Genetic Association between Intronic Variants in AS3MT and Arsenic Methylation Efficiency Is Focused on a Large Linkage Disequilibrium Cluster in Chromosome 10." *Journal of Applied Toxicology: JAT* 30 (3): 260–70. https://doi.org/10.1002/jat.1492.

Grignani, F., M. Valtieri, M. Gabbianelli, V. Gelmetti, R. Botta, L. Luchetti, B. Masella, et al.

2000. “PML/RAR Alpha Fusion Protein Expression in Normal Human Hematopoietic Progenitors Dictates Myeloid Commitment and the Promyelocytic Phenotype.” *Blood* 96 (4): 1531–37. https://www.ncbi.nlm.nih.gov/pubmed/10942402.

Heffelfinger, S. C., E. T. Sewell, and D. J. Danner. 1983. “Identification of Specific Subunits of Highly Purified Bovine Liver Branched-Chain Ketoacid Dehydrogenase.” *Biochemistry* 22 (24): 5519–22. https://doi.org/10.1021/bi00293a011.

Hodgkin, J., and T. Doniach. 1997. “Natural Variation and Copulatory Plug Formation in Caenorhabditis Elegans.” *Genetics* 146 (1): 149–64. https://www.ncbi.nlm.nih.gov/pubmed/9136008.

Hoonjan, Maneka, Vaibhav Jadhav, and Purvi Bhatt. 2018. “Arsenic Trioxide: Insights into Its Evolution to an Anticancer Agent.” *Journal of Biological Inorganic Chemistry: JBIC: A Publication of the Society of Biological Inorganic Chemistry* 23 (3): 313–29. https://doi.org/10.1007/s00775-018-1537-9.

Hughes-Fulford, M., Y. Chen, and R. R. Tjandrawinata. 2001. “Fatty Acid Regulates Gene Expression and Growth of Human Prostate Cancer PC-3 Cells.” *Carcinogenesis* 22 (5): 701–7. https://doi.org/10.1093/carcin/22.5.701.

Jia, Fan, Mingxue Cui, Minh T. Than, and Min Han. 2016. “Developmental Defects of Caenorhabditis Elegans Lacking Branched-Chain α-Ketoacid Dehydrogenase Are Mainly Caused by Monomethyl Branched-Chain Fatty Acid Deficiency.” *The Journal of Biological Chemistry* 291 (6): 2967–73. https://doi.org/10.1074/jbc.M115.676650.

Kang, H. M., N. A. Zaitlen, C. M. Wade, A. Kirby, D. Heckerman, M. J. Daly, and E. Eskin. 2008. “Efficient Control of Population Structure in Model Organism Association Mapping.” *Genetics* 178 (3): 1709–23. https://doi.org/10.1534/genetics.107.080101.

Kato, Masato, Jacinta L. Chuang, Shih-Chia Tso, R. Max Wynn, and David T. Chuang. 2005. “Crystal Structure of Pyruvate Dehydrogenase Kinase 3 Bound to Lipoyl Domain 2 of Human Pyruvate Dehydrogenase Complex.” *The EMBO Journal* 24 (10): 1763–74. https://doi.org/10.1038/sj.emboj.7600663.

Khairul, Islam, Qian Qian Wang, Yu Han Jiang, Chao Wang, and Hua Naranmandura. 2017. “Metabolism, Toxicity and Anticancer Activities of Arsenic Compounds.” *Oncotarget* 8 (14): 23905–26. https://doi.org/10.18632/oncotarget.14733.

Kim, Heesun, Takao Ishidate, Krishna S. Ghanta, Meetu Seth, Darryl Conte, Masaki Shirayama, and Craig C. Mello. 2014. “A Co-CRISPR Strategy for Efficient Genome Editing in Caenorhabditis Elegans.” *Genetics* 197 (4): 1069–80. https://doi.org/10.1534/genetics.114.166389.

Kniazeva, Marina, Quinn T. Crawford, Matt Seiber, Cun-Yu Wang, and Min Han. 2004. “Monomethyl Branched-Chain Fatty Acids Play an Essential Role in Caenorhabditis Elegans Development.” *PLoS Biology* 2 (9): E257. https://doi.org/10.1371/journal.pbio.0020257.

Kniazeva, Marina, Tanya Euler, and Min Han. 2008. “A Branched-Chain Fatty Acid Is Involved in Post-Embryonic Growth Control in Parallel to the Insulin Receptor Pathway and Its Biosynthesis Is Feedback-Regulated in C. elegans.” *Genes & Development* 22 (15): 2102–10. https://doi.org/10.1101/gad.1692008.

Large, Edward E., Wen Xu, Yuehui Zhao, Shannon C. Brady, Lijiang Long, Rebecca A. Butcher, Erik C. Andersen, and Patrick T. McGrath. 2016. “Selection on a Subunit of the NURF Chromatin Remodeler Modifies Life History Traits in a Domesticated Strain of Caenorhabditis Elegans.” *PLoS Genetics* 12 (7): e1006219. https://doi.org/10.1371/journal.pgen.1006219.

Li, Jiaojiao, Charles Packianathan, Toby G. Rossman, and Barry P. Rosen. 2017. “Nonsynonymous Polymorphisms in the Human AS3MT Arsenic Methylation Gene: Implications for Arsenic Toxicity.” *Chemical Research in Toxicology* 30 (7): 1481–91. https://doi.org/10.1021/acs.chemrestox.7b00113.

Luz, Anthony L., Tewodros R. Godebo, Dhaval P. Bhatt, Olga R. Ilkayeva, Laura L. Maurer, Matthew D. Hirschey, and Joel N. Meyer. 2016. “From the Cover: Arsenite Uncouples Mitochondrial Respiration and Induces a Warburg-like Effect in Caenorhabditis Elegans.” *Toxicological Sciences: An Official Journal of the Society of Toxicology* 152 (2): 349–62. https://doi.org/10.1093/toxsci/kfw093.

Luz, Anthony L., Tewodros R. Godebo, Latasha L. Smith, Tess C. Leuthner, Laura L. Maurer, and Joel N. Meyer. 2017. “Deficiencies in Mitochondrial Dynamics Sensitize Caenorhabditis Elegans to Arsenite and Other Mitochondrial Toxicants by Reducing Mitochondrial Adaptability.” *Toxicology* 387 (July): 81–94. https://doi.org/10.1016/j.tox.2017.05.018.

Luz, Anthony L., and Joel N. Meyer. 2016. “Effects of Reduced Mitochondrial DNA Content on Secondary Mitochondrial Toxicant Exposure in Caenorhabditis Elegans.” *Mitochondrion* 30 (September): 255–64. https://doi.org/10.1016/j.mito.2016.08.014.

Mandal, Badal Kumar, and Kazuo T. Suzuki. 2002. “Arsenic Round the World: A Review.” *Talanta* 58 (1): 201–35. https://doi.org/10.1016/S0039-9140(02)00268-0.

Murgo, A. J. 2001. “Clinical Trials of Arsenic Trioxide in Hematologic and Solid Tumors: Overview of the National Cancer Institute Cooperative Research and Development Studies.” *The Oncologist* 6 Suppl 2: 22–28. https://doi.org/10.1634/theoncologist.6-suppl_2-22.

Paix, Alexandre, Andrew Folkmann, Dominique Rasoloson, and Geraldine Seydoux. 2015. “High Efficiency, Homology-Directed Genome Editing in Caenorhabditis Elegans Using CRISPR-Cas9 Ribonucleoprotein Complexes.” *Genetics* 201 (1): 47–54. https://doi.org/10.1534/genetics.115.179382.

Paul, Somnath, Nilanjana Banerjee, Aditi Chatterjee, Tanmoy J. Sau, Jayanta K. Das, Prafulla K. Mishra, Partha Chakrabarti, Arun Bandyopadhyay, and Ashok K. Giri. 2014. “Arsenic-Induced Promoter Hypomethylation and over-Expression of ERCC2 Reduces DNA Repair Capacity in Humans by Non-Disjunction of the ERCC2-Cdk7 Complex.” *Metallomics: Integrated Biometal Science* 6 (4): 864–73. https://doi.org/10.1039/c3mt00328k.

Pettit, F. H., S. J. Yeaman, and L. J. Reed. 1978. “Purification and Characterization of Branched Chain Alpha-Keto Acid Dehydrogenase Complex of Bovine Kidney.” *Proceedings of the National Academy of Sciences of the United States of America* 75 (10): 4881–85. https://www.ncbi.nlm.nih.gov/pubmed/283398.

Ratnaike, R. N. 2003. “Acute and Chronic Arsenic Toxicity.” *Postgraduate Medical Journal* 79 (933): 391–96. https://doi.org/10.1136/pmj.79.933.391.

Ravenscroft, Peter, Hugh Brammer, and Keith Richards. 2009. *Arsenic Pollution : A Global Synthesis*. Chichester, U.K.: Wiley-Blackwell. http://www.worldcat.org/oclc/214285927?referer=xid.

Reed, L. J., and M. L. Hackert. 1990. “Structure-Function Relationships in Dihydrolipoamide Acyltransferases.” *The Journal of Biological Chemistry* 265 (16): 8971–74. https://www.ncbi.nlm.nih.gov/pubmed/2188967.

Schlebusch, Carina M., Lucie M. Gattepaille, Karin Engström, Marie Vahter, Mattias Jakobsson, and Karin Broberg. 2015. “Human Adaptation to Arsenic-Rich Environments.” *Molecular Biology and Evolution* 32 (6): 1544–55. https://doi.org/10.1093/molbev/msv046.

Schmeisser, Sebastian, Kathrin Schmeisser, Sandra Weimer, Marco Groth, Steffen Priebe, Eugen Fazius, Doreen Kuhlow, et al. 2013. “Mitochondrial Hormesis Links Low-Dose Arsenite Exposure to Lifespan Extension.” *Aging Cell* 12 (3): 508–17. https://doi.org/10.1111/acel.12076.

Shen, Shengwen, Xing-Fang Li, William R. Cullen, Michael Weinfeld, and X. Chris Le. 2013. “Arsenic Binding to Proteins.” *Chemical Reviews* 113 (10): 7769–92. https://doi.org/10.1021/cr300015c.

Shimko, Tyler C., and Erik C. Andersen. 2014. “COPASutils: An R Package for Reading, Processing, and Visualizing Data from COPAS Large-Particle Flow Cytometers.” *PloS One*

971 9 (10): e111090. https://doi.org/10.1371/journal.pone.0111090.
972 Spracklin, George, Brandon Fields, Gang Wan, Diveena Becker, Ashley Wallig, Aditi Shukla,
973 and Scott Kennedy. 2017. “The RNAi Inheritance Machinery of Caenorhabditis Elegans.”
974 *Genetics* 206 (3): 1403–16. https://doi.org/10.1534/genetics.116.198812.
975 Stýblo, Miroslav, Zuzana Drobná, Ilona Jaspers, Shan Lin, and David J. Thomas. 2002. “The
976 Role of Biomethylation in Toxicity and Carcinogenicity of Arsenic: A Research Update.”
977 *Environmental Health Perspectives* 110 Suppl 5 (October): 767–71.
978 https://www.ncbi.nlm.nih.gov/pubmed/12426129.
979 Tajima, F. 1989. “Statistical Method for Testing the Neutral Mutation Hypothesis by DNA
980 Polymorphism.” *Genetics* 123 (3): 585–95. https://www.ncbi.nlm.nih.gov/pubmed/2513255.
981 Team, R. Core. 2017. “R: A Language and Environment for Statistical Computing [Internet].
982 Vienna, Austria; 2014.”
983 Thé, H. de, C. Chomienne, M. Lanotte, L. Degos, and A. Dejean. 1990. “The t(15;17)
984 Translocation of Acute Promyelocytic Leukaemia Fuses the Retinoic Acid Receptor Alpha
985 Gene to a Novel Transcribed Locus.” *Nature* 347 (6293): 558–61.
986 https://doi.org/10.1038/347558a0.
987 Thompson, Owen A., L. Basten Snoek, Harm Nijveen, Mark G. Sterken, Rita J. M. Volkers,
988 Rachel Brenchley, Arjen Van’t Hof, et al. 2015. “Remarkably Divergent Regions Punctuate
989 the Genome Assembly of the Caenorhabditis Elegans Hawaiian Strain CB4856.” *Genetics*
990 200 (3): 975–89. https://doi.org/10.1534/genetics.115.175950.
991 Tomita, Akihiro, Hitoshi Kiyoi, and Tomoki Naoe. 2013. “Mechanisms of Action and Resistance
992 to All-Trans Retinoic Acid (ATRA) and Arsenic Trioxide (As2O 3) in Acute Promyelocytic
993 Leukemia.” *International Journal of Hematology* 97 (6): 717–25.
994 https://doi.org/10.1007/s12185-013-1354-4.
995 Tönjes, Martje, Sebastian Barbus, Yoon Jung Park, Wei Wang, Magdalena Schlotter, Anders M.
996 Lindroth, Sabrina V. Pleier, et al. 2013. “BCAT1 Promotes Cell Proliferation through Amino
997 Acid Catabolism in Gliomas Carrying Wild-Type IDH1.” *Nature Medicine* 19 (7): 901–8.
998 https://doi.org/10.1038/nm.3217.
999 Wang, Yunbiao, Anastasia N. Ezemaduka, Zhuheng Li, Zhanyan Chen, and Chuantao Song.
1000 2017. “Joint Toxicity of Arsenic, Copper and Glyphosate on Behavior, Reproduction and
1001 Heat Shock Protein Response in Caenorhabditis Elegans.” *Bulletin of Environmental*
1002 *Contamination and Toxicology* 98 (4): 465–71. https://doi.org/10.1007/s00128-017-2042-5.
1003 Watson, Emma, Lesley T. MacNeil, H. Efsun Arda, Lihua Julie Zhu, and Albertha J. M. Walhout.
1004 2013. “Integration of Metabolic and Gene Regulatory Networks Modulates the C. elegans
1005 Dietary Response.” *Cell* 153 (1): 253–66. https://doi.org/10.1016/j.cell.2013.02.050.
1006 Watts, Jennifer L., and Michael Ristow. 2017. “Lipid and Carbohydrate Metabolism in
1007 Caenorhabditis Elegans.” *Genetics* 207 (2): 413–46.
1008 https://doi.org/10.1534/genetics.117.300106.
1009 Wyatt, Lauren H., Anthony L. Luz, Xiou Cao, Laura L. Maurer, Ashley M. Blawas, Alejandro
1010 Aballay, William K. Y. Pan, and Joel N. Meyer. 2017. “Effects of Methyl and Inorganic
1011 Mercury Exposure on Genome Homeostasis and Mitochondrial Function in Caenorhabditis
1012 Elegans.” *DNA Repair* 52 (April): 31–48. https://doi.org/10.1016/j.dnarep.2017.02.005.
1013 Yeaman, S. J. 1989. “The 2-Oxo Acid Dehydrogenase Complexes: Recent Advances.”
1014 *Biochemical Journal* 257 (3): 625–32. https://www.ncbi.nlm.nih.gov/pubmed/2649080.
1015 Zdraljevic, Stefan, and Erik C. Andersen. 2017. “Natural Diversity Facilitates the Discovery of
1016 Conserved Chemotherapeutic Response Mechanisms.” *Current Opinion in Genetics &*
1017 *Development* 47 (September): 41–47. https://doi.org/10.1016/j.gde.2017.08.002.
1018 Zdraljevic, Stefan, Christine Strand, Hannah S. Seidel, Daniel E. Cook, John G. Doench, and
1019 Erik C. Andersen. 2017. “Natural Variation in a Single Amino Acid Substitution Underlies
1020 Physiological Responses to Topoisomerase II Poisons.” *PLoS Genetics* 13 (7): e1006891.
1021 https://doi.org/10.1371/journal.pgen.1006891.

1022 Zeidan, Amer M., and Steven D. Gore. 2014. “New Strategies in Acute Promyelocytic Leukemia:
1023 Moving to an Entirely Oral, Chemotherapy-Free Upfront Management Approach.” *Clinical*
1024 *Cancer Research: An Official Journal of the American Association for Cancer Research* 20
1025 (19): 4985–93. https://doi.org/10.1158/1078-0432.CCR-13-2725.
1026 Zhang, Xiao-Wei, Xiao-Jing Yan, Zi-Ren Zhou, Fei-Fei Yang, Zi-Yu Wu, Hong-Bin Sun, Wen-
1027 Xue Liang, et al. 2010. “Arsenic Trioxide Controls the Fate of the PML-RARalpha
1028 Oncoprotein by Directly Binding PML.” *Science* 328 (5975): 240–43.
1029 https://doi.org/10.1126/science.1183424.
1030 Zhu, Huanhu, Huali Shen, Aileen K. Sewell, Marina Kniazeva, and Min Han. 2013. “A Novel
1031 Sphingolipid-TORC1 Pathway Critically Promotes Postembryonic Development in
1032 Caenorhabditis Elegans.” *eLife* 2 (May): e00429. https://doi.org/10.7554/eLife.00429.

Supplemental Data:

Supplemental Data 1: Phenotype measurements for arsenic trioxide dose response data for four diverged *C. elegans* strains.
Supplemental Data 2: Raw RIAIL phenotype data used for linkage mapping
Supplemental Data 3: Assay-regressed RIAIL phenotype data used for linkage mapping
Supplemental Data 4: Control-regressed RIAIL phenotype data used for linkage mapping
Supplemental Data 5: Genome-wide LOD scores for animal length and brood size measurements from linkage mapping experiments.
Supplemental Data 6: Raw NIL and DBT-1 swap phenotype data.
Supplemental Data 7: Summarized NIL and DBT-1 swap phenotype data.
Supplemental Data 8: Control-regressed NIL and DBT-1 swap phenotype data.
Supplemental Data 9: NIL genotype data.
Supplemental Data 10: Raw wild-isolate data used for GWA mapping.
Supplemental Data 11: Summarized wild-isolate data used for GWA mapping.
Supplemental Data 12: Assay-regressed wild-isolate data used for GWA mapping.
Supplemental Data 13: Control-regressed wild-isolate data used for GWA mapping.
Supplemental Data 14: Processed brood size and animal length GWA mappings.
Supplemental Data 15: PCA traits for wild isolates used for GWA mappings.
Supplemental Data 16: Variance explained of principal components from wild-isolate data.
Supplemental Data 17: Processed PCA GWA mappings.
Supplemental Data 18: Fine-mapping of PC1 GWA mapping confidence interval.
Supplemental Data 19: PCA phenotype data for DBT-1 allele swap experiment.
Supplemental Data 20: Raw HTA data from C15iso rescue experiment.
Supplemental Data 21: Processed HTA data from C15iso rescue experiment.
Supplemental Data 22: *C. elegans* metabolite measurements.
Supplemental Data 23: Fraction of human cells with DBT1 edits.
Supplemental Data 24: Human cell line metabolite measurements
Supplemental Data 25: VCF used for Tajima's D calculation.
Supplemental Data 25b: VCF index used for Tajima's D calculation.
Supplemental Data 26: Tajima's D of GWA mapping confidence interval.
Supplemental Data 27: Isolation locations of strains used in GWA mapping.

Supplemental Tables:

Supplemental Table 1: Strains constructed for this study
Supplemental Table 2: Oligonucleotides used in this study

Supplemental Figures:

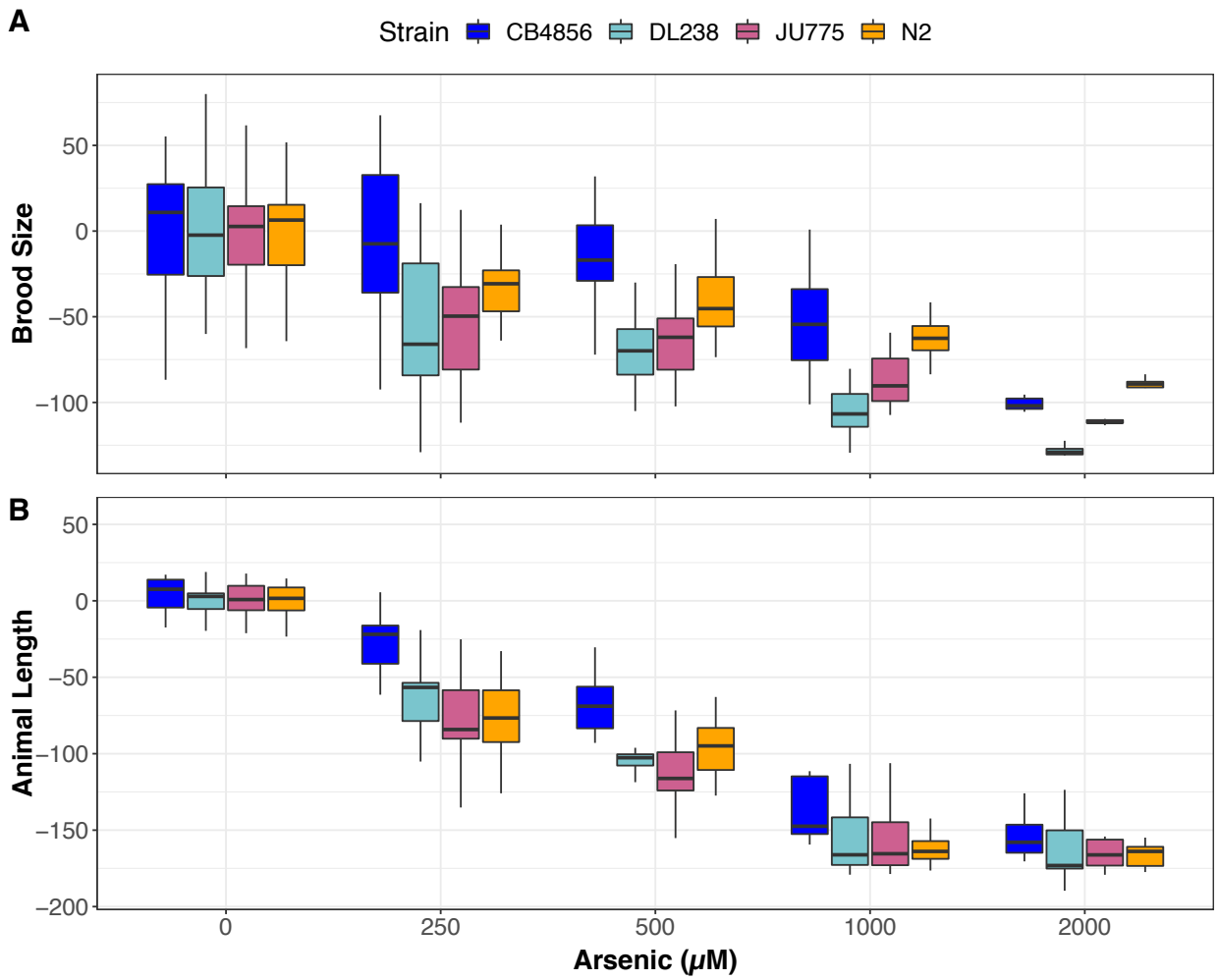

Supplemental Figure 1: Arsenic trioxide dose response of four diverged *C. elegans* strains

Arsenic trioxide concentration in μM is plotted on the x-axis and the (A) normalized brood size or (B) median progeny length are plotted on the y-axis. Y-axis values represent individual phenotypic measurements subtracted from the mean value in 0 μM arsenic trioxide. At least 15 replicates for each strain and condition are represented by Tukey box plots. Box plots are colored by strain (CB4856:blue, DL238:teal, JU775:pink, and N2:orange).

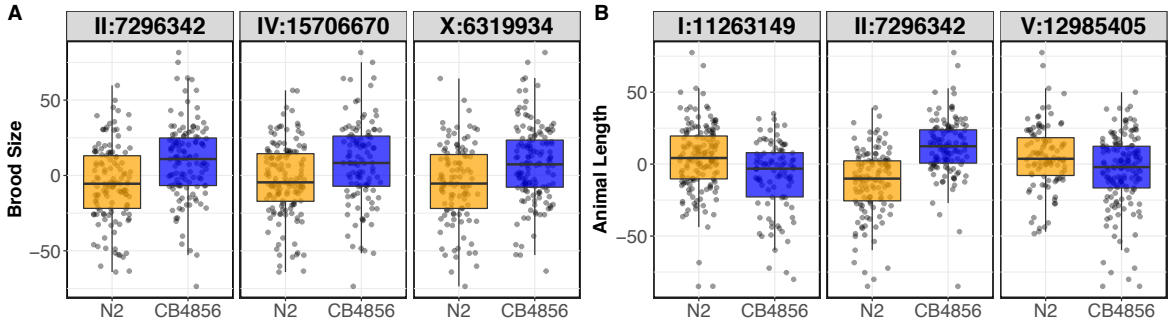

Supplemental Figure 2: RIAIL phenotypes from the linkage mapping experiment. Tukey box plots of regressed (A) brood sizes and (B) median animal lengths of the N2 and CB4856 RIAIL panel after exposure to arsenic trioxide. Each dot corresponds to the phenotype for a single RIAIL. The RIAILs are separated by the N2 (orange) or CB4856 (blue) genotype at the peak QTL positions identified by linkage mapping.

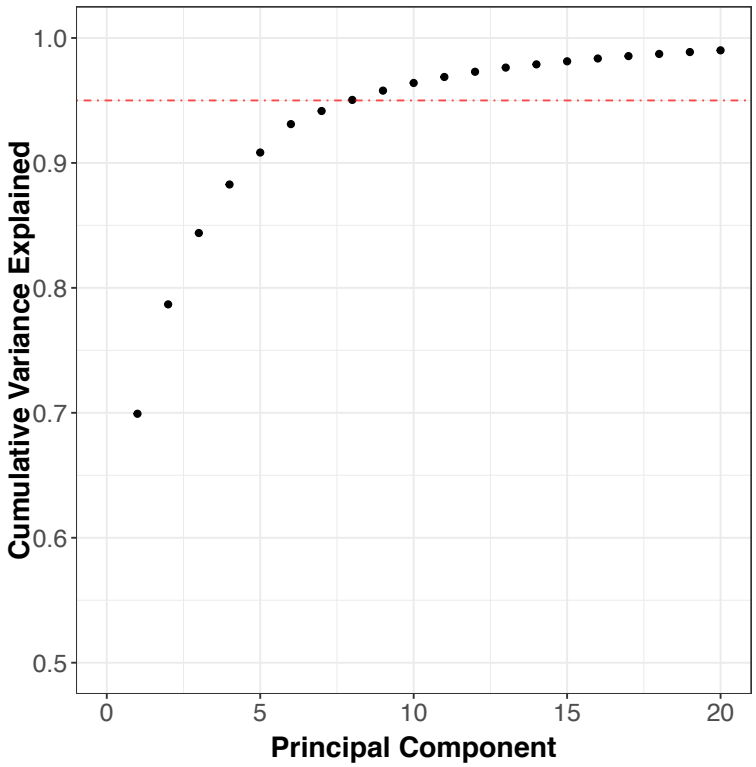

Supplemental Figure 3: Variance explained by principal components from GWA mapping experiment.
Principal component analysis was performed on 86 wild-isolate phenotypes measured by the COPAS BIOSORT after arsenic trioxide exposure. The x-axis corresponds to individual PCs. The cumulative proportion of variance explained by the first 20 principal components is shown on the y-axis. 95% of the phenotypic variance in this data set (red line) is captured by the first eight PCs.

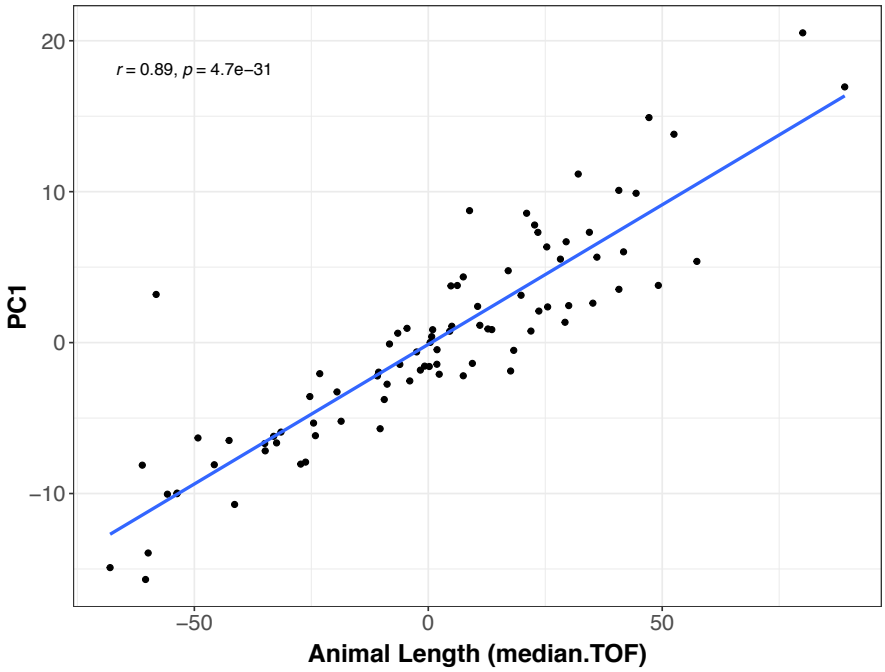

Supplemental Figure 4: Correlation between first principal component and animal length phenotypes

A scatter plot of the first principal component from PCA analysis of 67 phenotypes measured by the COPAS BIOSORT is plotted on the y-axis. The regressed median animal length is plotted on the x-axis. The Pearson correlation coefficient and the associated *p*-value of the correlation are inset in the upper left of the plot.

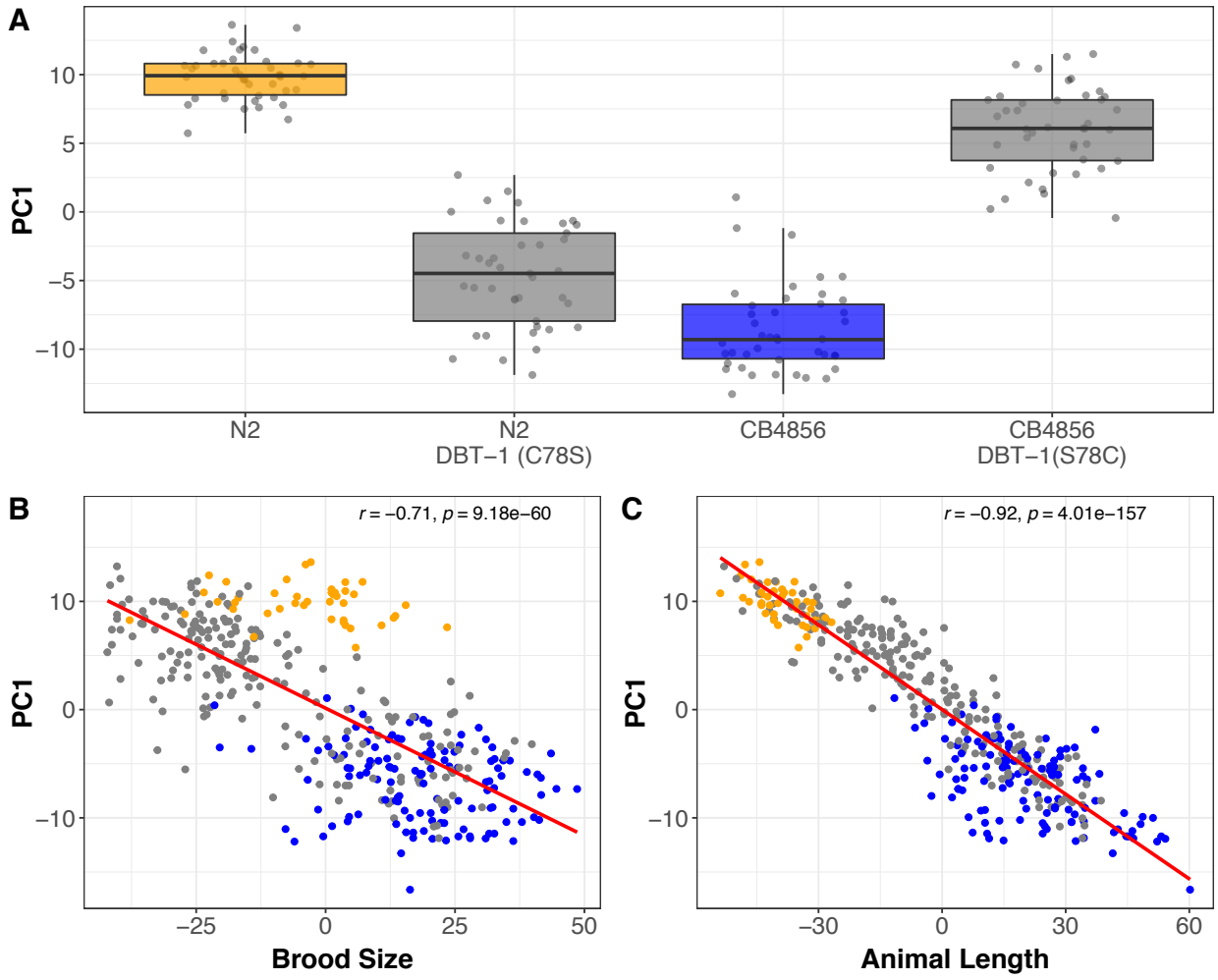

Supplemental Figure 5: Allele replacement strains recapitulate first principal component trait

(A) Tukey box plots of the first principal component generated by PCA on allele-replacement strain phenotypes measured by the COPAS BIOSORT after arsenic trioxide exposure are shown (N2, orange; CB4856, blue; allele replacement strains, gray). Labels correspond to the genetic background and the corresponding residue at position 78 of DBT-1 (C for cysteine, S for serine). Scatter plots showing a strong negative correlation between the first principal component and (B) brood size or (C) median animal length phenotypes from of the allele-replacement strains. Each dot corresponds to a strain replicate and are colored as in panel B. The Pearson correlation coefficient and the associated *p*-value of the correlation are inset in the upper right of the plot.

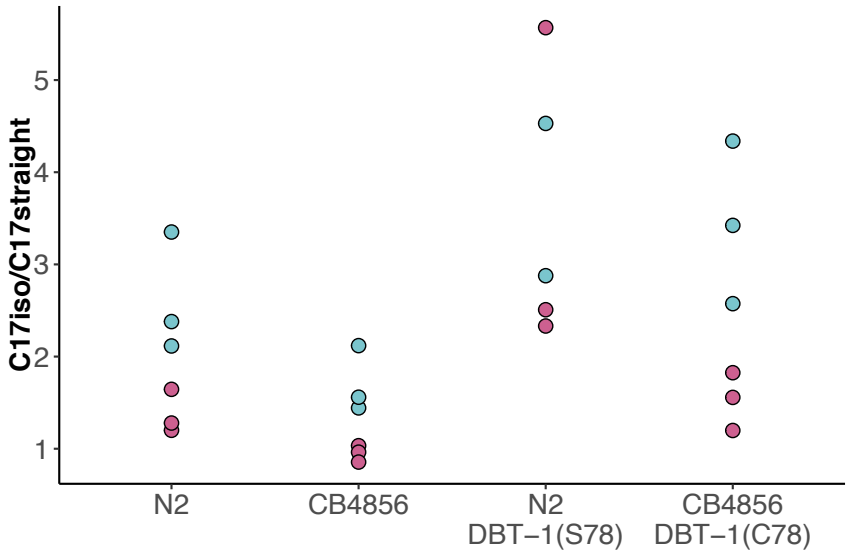

Supplemental Figure 6: C17ISO/C17straight ratios.
The ratio of C17ISO/C17straight-chain is plotted on the y-axis for three independent replicates of the N2, CB4856, and allele swap strains exposed to control (teal) or 100 µM arsenic trioxide (pink) conditions. The difference between N2 control and N2 arsenic trioxide conditions is significant (Tukey HSD *p*-value = 0.036), and the difference between CB4856 mock and arsenic conditions is (Tukey HSD *p*-value = 0.024). In The difference between N2 swap control and arsenic trioxide conditions is not statistically significant (Tukey HSD *p*-value = 0.89) and the difference between CB4856 swap mock and arsenic conditions is significant (Tukey HSD *p*-value = 0.024).

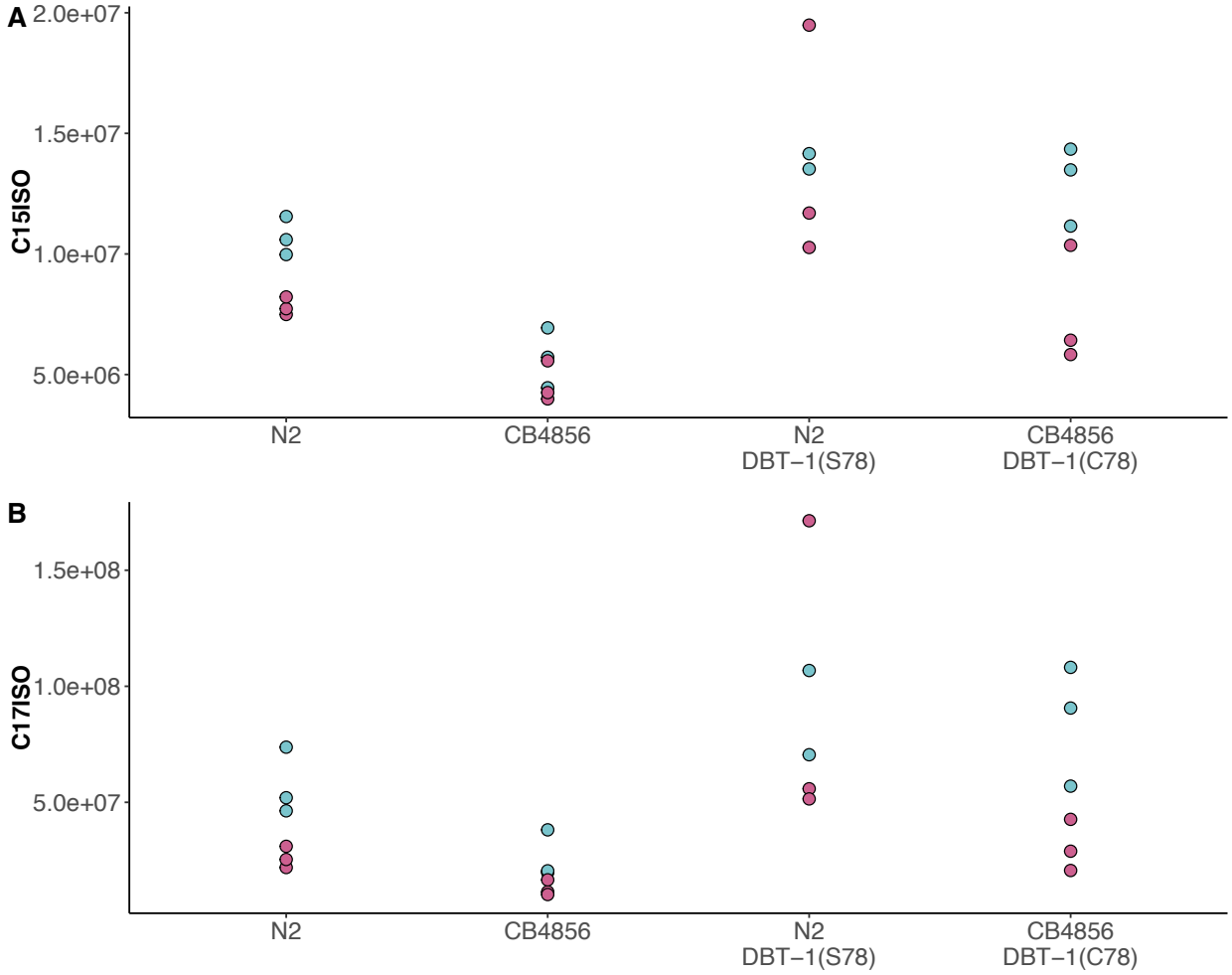

Supplemental Figure 7: Raw abundance of C15ISO and C17ISO.
The raw A) C15ISO and B) C17ISO is plotted on the y-axis for three independent replicates of the N2, CB4856, and allele swap strains exposed to control (teal) or 100 µM arsenic trioxide (pink) conditions. A) The difference between N2 control and N2 arsenic trioxide conditions is not significant (Tukey HSD *p*-value = 0.0046), but the difference between CB4856 mock and arsenic conditions is not (Tukey HSD *p*-value = 0.275). In The difference between N2 swap control and arsenic trioxide conditions is not statistically significant (Tukey HSD *p*-value = 0.99) and the difference between CB4856 swap mock and arsenic conditions is significant (Tukey HSD *p*-value = 0.033). B) The difference between N2 control and N2 arsenic trioxide conditions is not significant (Tukey HSD *p*-value = 0.024), but the difference between CB4856 mock and arsenic conditions is not (Tukey HSD *p*-value = 0.10). In The difference between N2 swap control and arsenic trioxide conditions is not statistically significant (Tukey HSD *p*-value = 0.94) and the difference between CB4856 swap mock and arsenic conditions is significant (Tukey HSD *p*-value = 0.029)

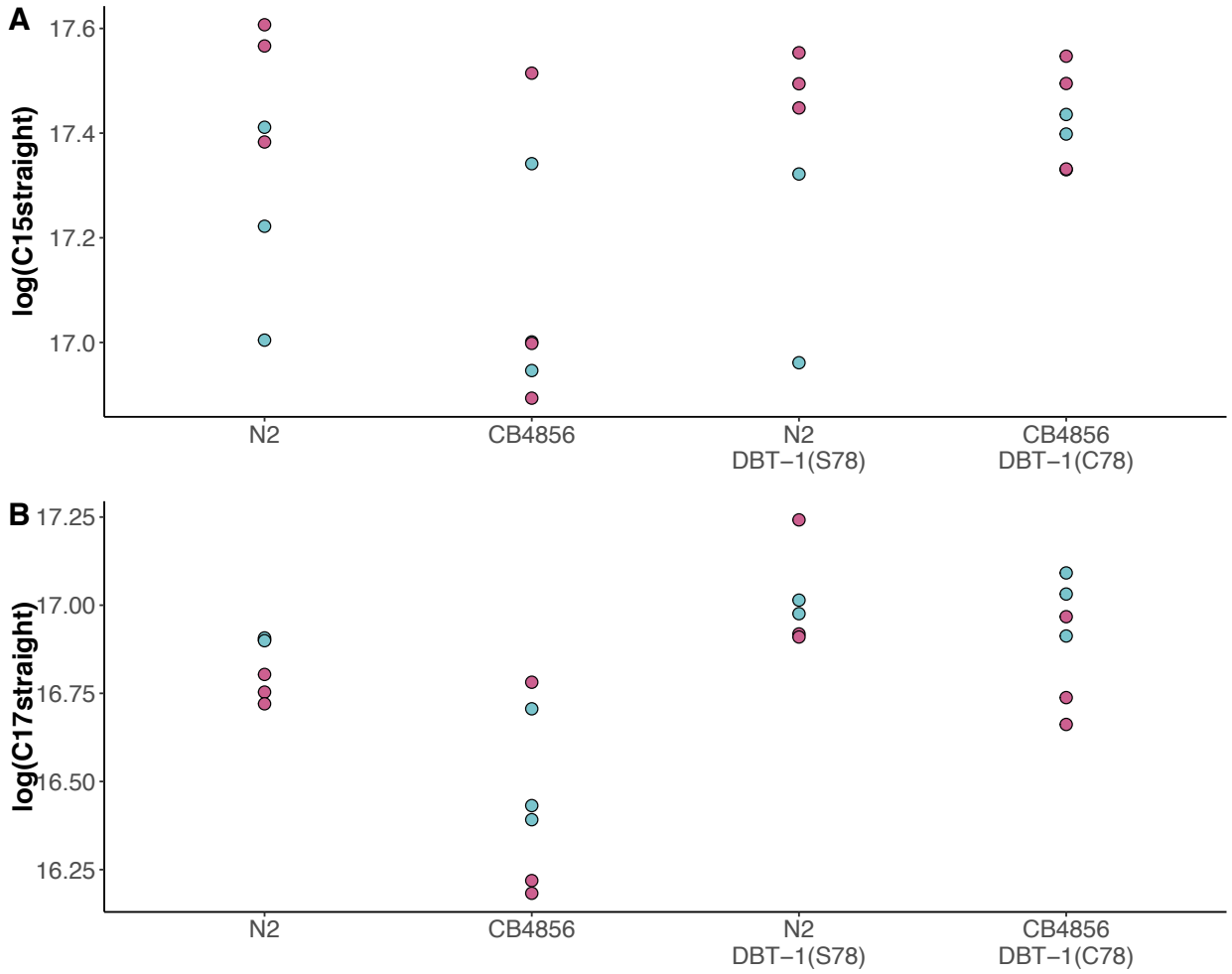

Supplemental Figure 8: C15 and C17 straight-chain metabolite levels.
The log-transformed raw abundance of A) C15 straight-chain and B) C17 straight-chain is plotted on the y-axis for three independent replicates of the N2, CB4856, and allele swap strains exposed to control (teal) or 100 µM arsenic trioxide (pink) conditions.

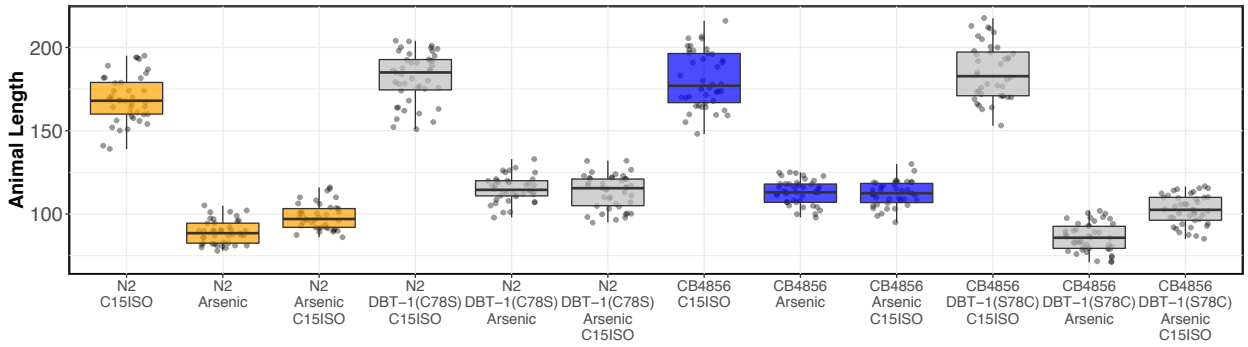

Supplemental Figure 9: Complete results from C15iso rescue experiment
Tukey box plots median animal length after C15ISO, arsenic trioxide, or arsenic trioxide and 0.64 µM C15ISO exposure are shown (N2, orange; CB4856, blue; allele replacement strains, gray). Labels correspond to the genetic background and the corresponding residue at position 78 of DBT-1 (C for cysteine, S for serine). Every pairwise strain comparison is significant except for the N2 DBT-1(S78) - CB4856 comparisons (Tukey's HSD *p*-value < 1.43E-6).

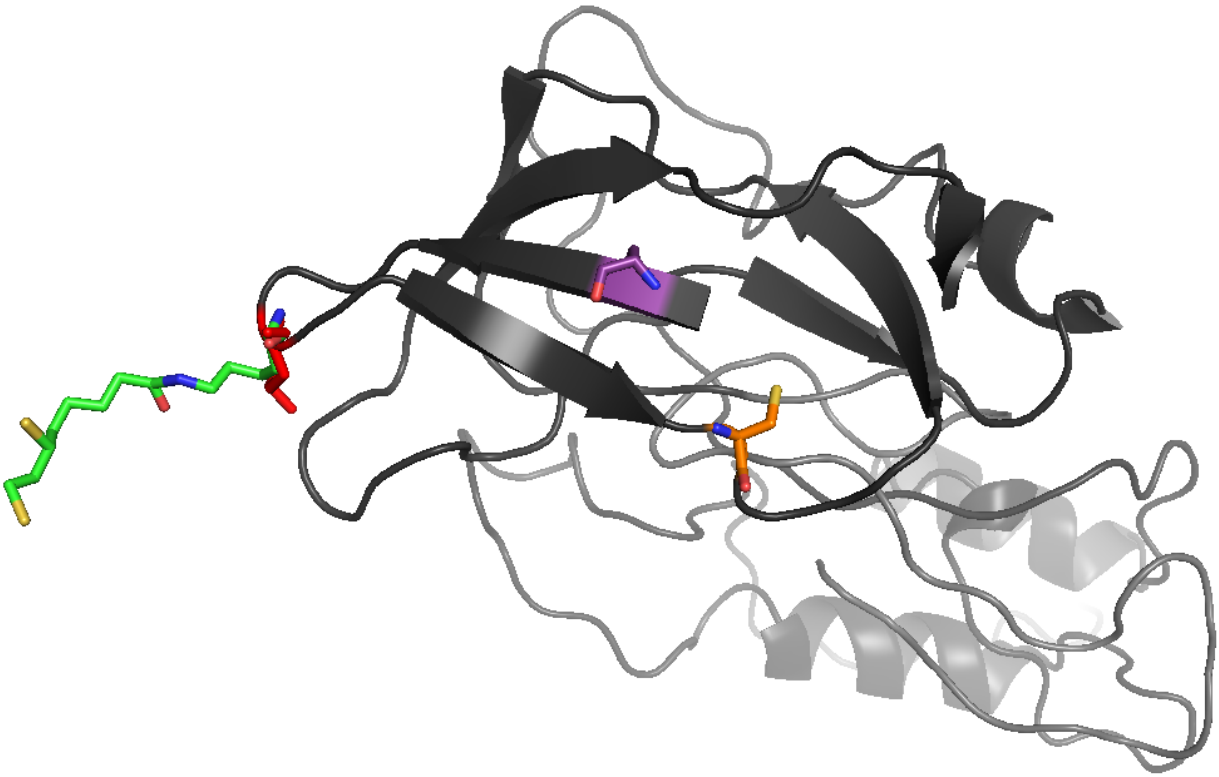

Supplemental Figure 10: Three-dimensional homology model of *C. elegans* DBT-1
A three-dimensional homology model of *C. elegans* DBT-1 (black) aligned to human pyruvate dehydrogenase lipoyl domain (PDB:1Y8N) is shown. The C78 residue that confers resistance to arsenic trioxide is highlighted in orange, and the C65 residue is highlighted in purple. The *C. elegans* K71 residue is highlighted in red, and the human lipoylated lysine is highlighted in green.

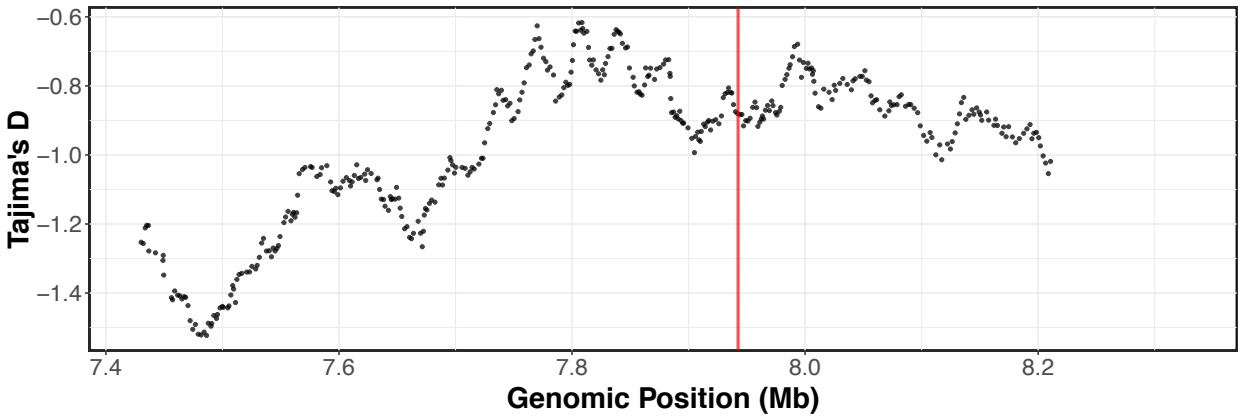

Supplemental Figure 11: Tajima's *D* across the arsenic trioxide QTL confidence interval Divergence, as measured by Tajima's D, is shown across the arsenic trioxide QTL confidence interval (II:7,430,000-8,330,000). The whole-genome SNV data set [24,49] was used for Tajima's D calculations. Window size for the calculations was 500 SNVs with a 10 SNV sliding window size. The vertical red line marks the position of the *dbt-1* locus.

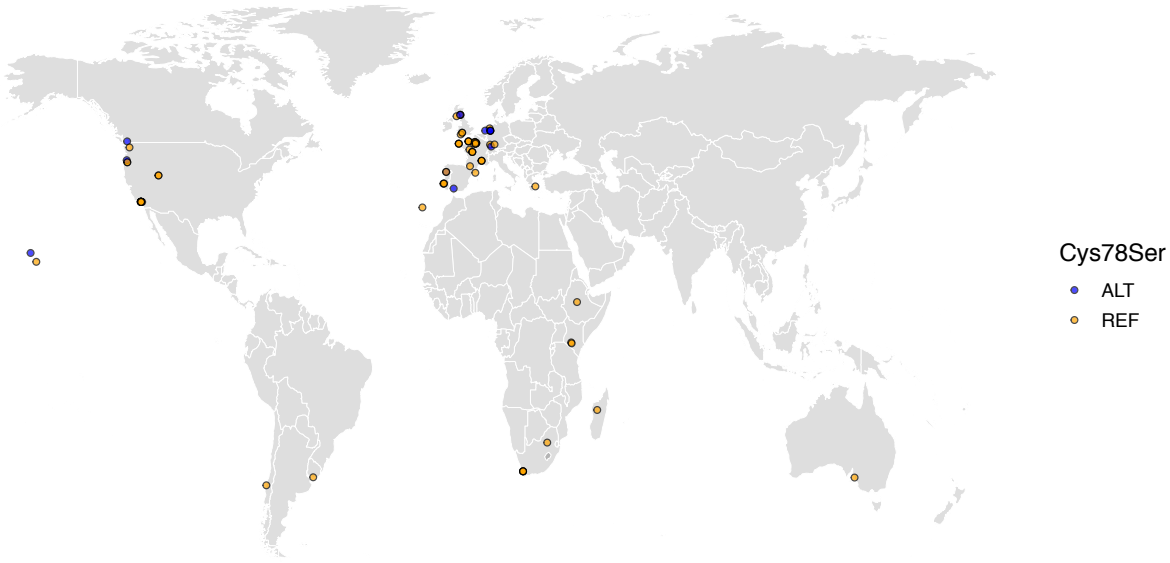

Supplemental Figure 12: The worldwide distribution of the DBT-1(C78S) allele
Cysteine (REF) is shown in orange and serine (ALT) is shown in blue. Latitude and longitude coordinates of sampling locations were used to plot individual strains on the map.